A high order moment method simulating evaporation and advection of a polydisperse liquid spray

Damien Kah, Frédérique Laurent, Marc Massot, Stéphane Jay

A high order moment method simulating evaporation and advection of a polydisperse liquid spray[☆]

D. Kah

Laboratoire EM2C - UPR CNRS 288, Ecole Centrale Paris, Grande Voie des Vignes, 92295 Chatenay-Malabry Cedex, France, and IFP - Energies Nouvelles, 1 et 4 avenue de Bois Préau 92852 Rueil-Malmaison, France

F. Laurent, M. Massot[*]

Laboratoire EM2C - UPR CNRS 288, Ecole Centrale Paris, Grande Voie des Vignes, 92295 Chatenay-Malabry Cedex, France.

S. Jay

IFP - Energies Nouvelles, 1 et 4 avenue de Bois Préau 92852 Rueil Malmaison, France

Abstract

In this paper, we tackle the modeling and numerical simulation of dilute gas-droplet and gas-particle flows for which polydispersity description is of paramount importance. Starting from a kinetic description for point particle experiencing transport either at the carrier phase velocity for aerosols or at their own velocity for more inertial particles, we focus on an Eulerian high order moment method in size and consider a system of partial differential equations (PDEs) on a vector of successive size moment of order 0 to N, $N > 2$, over a compact size interval. There exists a stumbling block for the usual approaches using high order moment method resolved with high order finite volume method: the transport algorithm does not preserve the moment space Indeed, reconstruction of moments by polynomials inside computational cells coupled to the evolution algorithm can create N-dimensional vectors which fail to be moment vectors: it is impossible to find a size distribution for which there are the moments. To achieve still a robust scheme, one possibility is to use projections onto the moment space but this leads to a substantial loss of accuracy and performance. We thus propose a new approach as well as an algorithm which is second order in space and time with very limited numerical diffusion and allows to accurately describe the advection process and naturally preserves the moment space. By coupling this approach to a recently designed algorithm for evaporation which also preserves the moment space, polydispersity is accounted for in the evaporation and advection process, very accurately and at a very reasonable computational cost. We show that such an approach is very competitive compared to multi-fluid approches where the size phase space is discretized into several sections and low order moment methods are used in each section. Two 2D test-cases are presented: Taylor-Green vortices and turbulent free jets, where the accuracy and efficiency of the approach are assessed.

Key words: Polydisperse sprays, aerosols, high order moment method, moment space, canonical moments, Eulerian multi-fluid model, Maximum Entropy reconstruction, kinetic finite volume schemes
2000 MSC: 35Q35, 65M12, 65M99, 76T10

[☆]This work was supported by a Young Investigator Award for M. Massot (ANR-05-JCJC-0013 - jéDYS - 2005-2009) from ANR in France (National Research Agency) and by a CNRS financial support (PEPS "Projet Exploratoire Pluridisciplinaire" 2007-2009, from the ST2I and MPPU Departments of CNRS, coordination: A. Bourdon and F. Laurent) .
[*]Corresponding author - marc.massot@em2c.ecp.fr

1. Introduction

The study of multi-phase flow is of major importance and interest in many fields such as combustion, chemical engineering [35], rocket booster propulsion [11, 12] and atmospheric studies [41]. A key example involving this kind of flow is fuel injection in internal combustion engines. The fuel is typically stored as a liquid phase and injected at high pressures (up to 2000 bars) into a gas-filled combustion chamber. Due to the interactions with the surrounding gas, the dense liquid core atomizes and eventually results in a dilute droplet cloud called spray which is polydisperse, in a region located downstream of the injector and where combustion is taking place. The spatial topology of the fuel mass fraction is a direct consequence of the turbulent dispersion and evaporation of the spray in that region and is strongly related to size distribution since droplet dynamics and evaporation are conditioned on droplet size. The spray dynamics thus governs the resulting combustion regimes, and therefore has a strong influence on the key undesirable by-products of an engine, such as pollutants and soots. Since experimental measurements of various combustion chamber configurations for design purposes can be very expensive, computational models for multi-phase flows have recently become widely studied. Therefore, it is of great interest to design reliable models for such polydisperse sprays flow, as well as numerical methods which are as accurate as possible, but also tractable for large scale computations on parallel architectures. It is for this purpose that the scope of this work is the introduction of a new numerical approach based on high order size moment methods and on a rigorous mathematical background for dilute particulate flow regions which is both stable and computationally advantageous.

Dilute gas-droplet and gas-particle flows are typically described by a kinetic equation modeling clouds of point particles, represented by its number density function (NDF), through transport, particle-fluid interactions, and eventually particle-particle interactions in the framework of moderately dense cases. In most cases the sprays are polydisperse and experience size evolution due to evaporation; in such configurations, typical of reactive flows, the description of the droplet/particle size distribution is of paramount importance. The Knudsen number is assumed to be high so that the collision between particles can be neglected. Additionally, the particle Stokes number based on some typical gas flow time can range from $\mathrm{St} << 1$ to $\mathrm{St} \approx 1$. This includes two different types of particles. The class corresponding to $\mathrm{St} << 1$ is called aerosol. They are potentially sensitive to the Brownian motion of the gas and are transported at the gaseous flow velocity. For higher Stokes number ($\mathrm{St} \approx 1$), the Brownian motion of gas molecules has no impact any more on the particles, which have their own inertia and dynamics and interact with the gas through a drag force. This class is called spray. Moreover, an effective model for dilute gas-particles flow must include both the kinetic description for the particle phase and a coupled momentum balance equation for the gas phase. Nevertheless, the principal modeling challenge is the simulation of polydispersity and dynamics of the particle population. Therefore, in this contribution, we will consider one-way coupling for comparison purposes, i.e. we will assume that the fluid velocity is given and influences the spray dynamics and evaporation. Nevertheless, the extension to two-way coupling is straightforward and all the easier since the two phases are described by a Eulerian model.

Since the direct resolution of the kinetic equation is often intractable due to the large number of independent variables, stochastic Lagrangian methods "discretize" the NDF into "parcels", the dynamics of which is integrated. This approach has been widely used and has been shown to be efficient in numerous cases (see example [15] and references herein). While quite accurate, its main drawback is the coupling of an Eulerian description for the gaseous phase to a Lagrangian description of the disperse phase, thus offering limited possibilities of vectorization/parallelization. Besides, as in any statistical approach, Lagrangian methods require a relatively large number of parcels to control statistical noise, and thus are computationally expensive, especially for polydisperse unsteady flows. An alternative to the Lagrangian approach is a Eulerian moment method. The closure of the velocity moments conditioned on size is classical and conducted through a usual hydrodynamic limit leading to an equilibrium velocity distribution, i.e. Maxwell-Boltzmann distribution up to zero temperature in the framework of direct numerical simulation [25, 7, 22]. Once a closure has been chosen in terms of velocity moments conditioned on droplet size [25], there are two options available for capturing the dynamics in the size phase space. One can either rely on size phase space discretization, with low order size moments in each section, as done in the multi-fluid approach developed in [9, 7, 25] from [21]. The multi-fluid model considers only one size moment which accounts for the liquid mass on small intervals of the size phase space called sections.

Formally, the disperse phase is composed of several fluids exchanging among each other and with the gas, through evaporation mass and momentum fluxes. This model has been shown to yield simple transport algorithms for transport in physical space in [9, 8, 7] implemented on parallel architectures [17, 18]. However, the cost of the discretization in size phase space is high and still results in numerical diffusion since the method is first order in size discretization width [24]. Therefore, in terms of computational cost, the possibility of high order moment method considering only one size section is very attractive.

At present, several high order moment methods have been designed. The first one consists of solving the evolution of moments of a presumed NDF (assumed as a log-normal law) [34]. Presumably, this seems very attractive since knowing *a priori*, the profile of the NDF makes its reconstruction from the moments much easier. However, this assumption is restrictive in terms of the coverage of the physical processes. Moreover, this approach leads to serious numerical instabilities thus preventing its use for the treatment of an evaporating spray, since during the computation, a log-normal distribution function might not be reconstructed from the moment set. The second method uses Direct Quadrature Method of Moment (DQMOM) [27] wherein equations are directly written on the quadrature weights and abscissas which describe the reconstructed distribution function having the same moments [15]. Contrary to the first one, this method is robust but is not able to accurately predict the evaporating flux in every case [15]. Consequently, further studies have been undertaken and have lead to a proper treatment of the evaporation term. The high order moment method together with the associated numerical scheme explained in [30] is a breakthrough in terms of accuracy, and can be effectively used for quantitative predictions of an evaporating spray. This has been developed in the context of a homogeneous spray, i.e. without transport in physical space. In this contribution, we focus on transport in physical space and on the treatment of the particle size distribution by high order moment method in the size dimension, where the particle size spans a compact interval, in the context of finite volume methods. We aim at transporting a vector of integer and successive size moment up to order N, $N > 2$.

There exists a stumbling block for the usual approaches using high order moment method resolved with at least second order finite volume method: the transport algorithm does not preserve the moment space, that is, spatial reconstruction of moments by polynomials inside computational cells coupled to the evolution algorithm can create N-dimensional vectors which fail to be moment vectors: it is impossible to find a size distribution for which there are the moments. In fact two difficulties arise. The first one concerns the reconstruction of the moments in order to keep the integrity of the moment set. It has been seen that for a high order in space scheme, an independent reconstruction of each moment does not insure that the moment space is preserved [41, 31]. Besides, a second difficulty concerns the computation of the fluxes from the reconstructed quantities. If an approximate time solver is used (Explicit Euler, Runge-Kutta), the fluxes computation will introduce troncature errors for non constant reconstructions, and the preservation of the moment space will not be guaranteed any more, even if there were no problem in the reconstruction step. To achieve still a robust scheme, one possibility is to use projections onto the moment space but this leads to a substantial loss of accuracy and performance.

We thus propose a new approach as well as an algorithm which is second order in space and time with low numerical diffusion which allows to accurately describe the advection process and naturally guarantees that the vector always belongs to the moment space if the initial solution itself belongs to the moment space. We tackle both aerosols which are transported by the velocity of the carrier flow as well as more inertial particle/droplets which have their own velocity field. The required ingredients are a reconstruction of the independent canonical moments, which are well-suited since there are transported quantities, as well as the use of a time solver based on an exact resolution of the PDE in time, leading to the fact that the fluxes introduce no troncature error with respect to the spatial reconstruction. An exact computation of the fluxes is obtained using the fact that the equations on moments can be derived from a kinetic equation as originally proposed in Bouchut [2]. By coupling this approach to a recently designed algorithm for evaporation which also preserves the moment space [30], polydispersity is accounted for in the evaporation and advection process, very accurately and at a very reasonable computational cost. We show that such an approach is very competitive compared to multi-fluid approches where the size phase space is discretized into several sections and low order moment methods are used in each section. Two 2D test-cases are presented: Taylor-Green vortices and turbulent free jets. We thus show the achievements of the present contribution as well as its adequation to more complex configurations on parallel architectures.

The remainder of the paper is organized as follows. In Section 2 the kinetic equation for both

the class of aerosol and sprays is presented and the system of PDEs for high order size moment in the two cases obtained; furthermore, the main properties of the moment space as well as canonical moments are introduced as well as the main mathematical properties of the systems of PDEs which will be useful in order to design the new transport algorithm. Section 3 contains the development of the kinetic-based finite volume numerical scheme for the transport in physical space, wherein reconstruction on canonical moments are used for the computation of the fluxes. In Section 4 the essential points of the numerical scheme for the treatment of the evaporation term are highlighted. Section 5 is first dedicated to an application example designed to validate the numerical method and algorithm as well as its implementation. Then, two 2D configurations of the gaseous flow field are considered, a Taylor Green steady and an unsteady weakly turbulent free jet. It allows us to compare the newly designed algorithm to the multi-fluid model in terms of accuracy and computational cost.

2. High order moment model and associated properties

This section is dedicated to the derivation of the system of PDEs on particle size and velocity moments from the kinetic equation governing the evolution of the NDF. The cases of aerosol and sprays are treated separately as they lead to different systems of PDEs, even if they rely on the same basis at the kinetic level. Since we consider successive integer order size moments of the NDF, the structure of the moment space as well as the canonical moments are presented and the main properties of the two systems of PDEs involving these vectors of moments are analyzed. This is essential since it will induce the choices in terms of numerical methods in the following section. Moreover, the closure of velocity moments for sprays introduces the pressureless gas formalism, the influence of which is briefly described.

2.1. Fundamental modeling at the kinetic level

The dilute droplet flow is described by a NDF $f(t,\boldsymbol{x},S,\boldsymbol{v})$, such that $f(t,\boldsymbol{x},S,\boldsymbol{v})\mathrm{d}\boldsymbol{x}\mathrm{d}S\mathrm{d}\boldsymbol{v}$ represents the probable number of particles located in $\boldsymbol{x}=(x_1,\dots,x_d)$, where d is the dimension of the physical space), with size S, and velocity $\boldsymbol{v}$. As the particles are assumed to be spherical, we choose the particle surface to describe the size. We could have also chosen to work with their radius, r or their volume, V, all corresponding NDF being linked by the relation $f(t,\boldsymbol{x},r,\boldsymbol{v})dr = f(t,\boldsymbol{x},S,\boldsymbol{v})\mathrm{d}S = f(t,\boldsymbol{x},V,\boldsymbol{v})\mathrm{d}V$. In the applications targeted in this paper, the particles/droplets evolve through evaporation and interaction with gas molecules which results in transport in physical space, drag and eventually Brownian motion. The kinetic equation verified by the NDF is a Fokker-Planck based equation:

$$\partial_t f + \partial_{\boldsymbol{x}}(\boldsymbol{v}f) - \partial_S(Rf) = \beta\partial_{\boldsymbol{v}}[((\boldsymbol{v}-\boldsymbol{u}_g)f + \frac{\boldsymbol{Q}}{\beta}\partial_{\boldsymbol{v}}f)]. \tag{1}$$

The second term of the left hand side represents transport in physical space, whereas the third term accounts for the evaporation of the droplets. The terms of the right hand side stand for Stokes drag force and Brownian motion due to the interaction of the droplets with the gas molecules. The evaporation rate, R, is the rate of decrease of the droplet surface, β^{-1} is the relaxation time of the particles, $\boldsymbol{u}_g$ is the gas velocity, $\mathbf{Q}$ is the matrix of the temporal correlation of accelerations, $\boldsymbol{F}=(F_1,F_2,F_3)^t$ due to Brownian motion in three dimensions, $Q_{ij}(t)=\int_0^\infty F_i(t)F_j(t+\tau)\,d\tau$. We introduce dimensionless variables:

$$t' = \frac{tU_0}{L_0},\quad x' = \frac{x}{L_0},\quad S' = \frac{S}{S_0},\quad \boldsymbol{v}' = \frac{\boldsymbol{v}}{U_0},\quad \boldsymbol{u}_g' = \frac{\boldsymbol{u}_g}{U_0},\quad f' = f\frac{U_0^3L_0^3S_0}{N_0},$$
$$\tau_g = \frac{L_0}{U_0},\quad \mathrm{St} = \frac{U_0\beta^{-1}}{L_0},\quad K = \frac{RL_0}{S_0U_0},\quad \boldsymbol{\sigma} = \frac{\mathbf{Q}\beta^{-1}}{U_0^2},$$

where L_0 is a reference length, U_0 a reference velocity, S_0 the maximum droplet size, N_0 a reference number density. The characteristic time of the particles is τ_g, St the Stokes number, K the nondimensional evaporation rate, $\boldsymbol{\sigma}$ the velocity variance at equilibrium of the particles due to Brownian motion. Written in terms of dimensionless quantities, the Fokker-Planck equation reads:

$$\partial_t' f' + \partial_{\boldsymbol{x}'}(\boldsymbol{v}'f') - \partial_S'(Kf') = \frac{1}{\mathrm{St}}\partial_{\boldsymbol{v}'}[(\boldsymbol{v}'-\boldsymbol{u}_g')f' + \boldsymbol{\sigma}\partial_{\boldsymbol{v}'}f']. \tag{2}$$

In the following, for the sake of legibility, we will write the dimensionless quantities without the prime sign. Before investigating the system of macroscopic partial differential equation on the size moments which is at the heart of the present contribution, let us first take the moments in velocity conditioned on size and differentiate between two cases, depending on the range of the Stokes number, aerosols for very small Stokes numbers and sprays for moderate Stokes numbers.

2.1.1. Aerosol

We first consider the aerosol dynamics for which no terms in Eq. (2) can be neglected, that is the effect of the collision of the surrounding gas molecules at thermodynamical equilibrium on the aerosol particles/droplets results in a significative velocity variance compared to the slip velocity.

As it is classical in statistical physics, a Langevin equation can be associated to the previous Fokker-Planck equation, which in the "viscous limit" or for large times compared to β^{-1} when the inertial term in the equation of motion can be disregarded, reduces to a spatial diffusion as studied in the original works of Einstein and Smoluchowski [5]. Since we rather work with NDF and consider the equation (2) as the fundamental model of our particles/droplets, we will obtain the spatially diffusive regime as a singular perturbation using a Chapman-Enskog type of expansion. For the sake of clarity, let us thus rewrite Eq. (2) as :

$$\partial_t f + \partial_{\boldsymbol{x}}(\boldsymbol{v}f) - \partial_S(Kf) = \frac{1}{\epsilon}J(f), \qquad J(f) = \partial_{\boldsymbol{v}}[(\boldsymbol{v}-\boldsymbol{u}_g)f + \boldsymbol{\sigma}\partial_{\boldsymbol{v}}f]. \tag{3}$$

The differential operator $J(f)$ appears as a singular perturbation of Eq. (3), in the case $\epsilon \to 0$. The NDF is solved using a Chapman-Enskog development (see classical references of kinetic theory of gases [20, 13, 6, 39]), that is to say that f is decomposed into powers of ϵ:

$$f = f^{(0)} + \epsilon f^{(0)}\phi^{(1)} + \epsilon^2 f^{(0)}\phi^{(2)} + ... \tag{4}$$

where each order of ϵ is recursively solved from the lower orders of f. Moreover, we look at various order perturbations which leave unchanged the macroscopic quantities. In this problem, the sole macroscopic quantity associated to the one-dimensional subspace of invariant of operator J is the total droplet number $\int J(f)\,\mathrm{d}\boldsymbol{v} = 0$, so each $\phi^{(k)}$ verifies $\int f^{(0)}\phi^{(k)} = 0$.

The 0^{th} order term of f, $f^{(0)}$, is the solution of $J(f^{(0)}) = 0$, which is the kernel of operator J. It can be easily proven that f^0 is a Maxwell-Boltzmann distribution, which reads:

$$f^{(0)} = n(t,\boldsymbol{x},S)\frac{1}{\sqrt{(2\pi)^3 det(\boldsymbol{\sigma})}}\exp(-\boldsymbol{C}^t\boldsymbol{\sigma}^{-1}\boldsymbol{C}), \qquad \boldsymbol{C} = \boldsymbol{v}-\boldsymbol{u}_g. \tag{5}$$

The terms of higher order with respect to ϵ in the Chapman-Enskog expansion (4) satisfy differential equations, the right-hand side of which involve the lower order terms and the kernel of which is associated to the only macroscopic quantity conserved by the J operator, that is total number density of particles. In this context, we end up with a self-adjoint compact differential operator with a one dimensional kernel in the proper Hilbert space, for which a Fredholm alternative guarantees the resolvability of $\phi^{(1)}$ and leads to the macroscopic equation of order 0 in ϵ :

$$\partial_t n + \partial_{\boldsymbol{x}}(n\boldsymbol{u}_g) - \partial_S(Kn) = 0. \tag{6}$$

Extending the resolution of Eq.(3) to the first order of ϵ leads to the following equation:

$$\partial_t n + \partial_{\boldsymbol{x}}(n\boldsymbol{u}_g) - \partial_S(Kn) = \epsilon\partial_{\boldsymbol{x}}\big(\boldsymbol{\sigma}\partial_{\boldsymbol{x}}n - n(D_t\boldsymbol{u}_g)\big), \qquad D_t\boldsymbol{u}_g = \partial_t\boldsymbol{u}_g + (\boldsymbol{u}_g.\partial_{\boldsymbol{x}})\boldsymbol{u}_g, \tag{7}$$

where the flux at first order in ϵ delivers a diffusion term as well as an acceleration term which can be related to a normalized pressure gradient in the framework of an incompressible flow for the gaseous phase and which will not be considered in the following for the sake of clarity of the exposition. This allows us to write the following equation on the total number density conditioned on size, $n(t,\boldsymbol{x},S)$, called the Smoluchowski equation [19, 5]:

$$\partial_t n + \partial_{\boldsymbol{x}}(\boldsymbol{u}_g n) - \partial_S(Kn) = \partial_{\boldsymbol{x}}(\boldsymbol{D}\partial_{\boldsymbol{x}}n), \tag{8}$$

where the diffusion operator reads $\boldsymbol{D} = \epsilon\boldsymbol{\sigma}$ and which is valid for time scales large compared to β^{-1}.

2.1.2. Spray

In the case of spray particles, their Stokes regime (St ≈ 1) is such that their dynamics is mainly governed by the drag term and the developing slip velocity with respects to the gas, and, in most cases, for the considered time scales, they are not influenced by the small scale fluctuations of the Brownian motion. Thus f satisfies the following kinetic equation, called Williams-Boltzmann equation [40]:

$$\partial_t f + \partial_{\boldsymbol{x}}(\boldsymbol{v} f) - \partial_S(Kf) + \partial_{\boldsymbol{v}}\left(\frac{1}{\mathrm{St}}(\boldsymbol{u}_g - \boldsymbol{v})f\right) = 0. \tag{9}$$

Contrary to the previous case, the drag term is not a singular perturbation in Eq. (9). So an equation on n, the number density, but also on $n\,u = \int f\,v\,dv$ which is the particle mean momentum conditioned on size, have to be derived. These equations are obtained by taking the velocity moment of order 0 and 1 of Eq. (9):

$$\partial_t n + \partial_{\boldsymbol{x}}(n\boldsymbol{u}) - \partial_S(Kn) = 0, \tag{10}$$

$$\partial_t(n\boldsymbol{u}) + \partial_{\boldsymbol{x}}(n\boldsymbol{u}\otimes\boldsymbol{u} + n\boldsymbol{P}) - \partial_S(Kn\boldsymbol{u}) - n\frac{\boldsymbol{u}_g - \boldsymbol{u}}{\mathrm{St}} = 0, \tag{11}$$

where $n\,\boldsymbol{P} = \int(\boldsymbol{v}-\boldsymbol{u})\otimes(\boldsymbol{v}-\boldsymbol{u})f\,\mathrm{d}v$ is the particle pressure tensor. Contrary to the previous case where f relaxes to a Maxwell-Boltzmann distribution, in this case this closure is not obtained naturally from Eq. (9) as a relaxation toward equilibrium. A hypothesis on the velocity distribution has to be made in order to obtain a closed equation on the total number density conditioned on size, $n(t,x,S)$. Following the example of what is done in the multi-fluid model [21, 25, 7], we suppose that there is no dispersion around the mean velocity. In other terms, we "project" f on a distribution with a single velocity conditioned on size: $f(t,\boldsymbol{x},S,\boldsymbol{v}) = n(t,\boldsymbol{x},S)\delta(\boldsymbol{v}-\boldsymbol{u}(t,\boldsymbol{x},S))$, leading to $\boldsymbol{P}=0$. This assumption is fully legitimate for small Stokes numbers, as $\boldsymbol{u}\approx\boldsymbol{u}_g$ in this case. Nevertheless even if St ≈ 1, where physically some velocity slip may occur, this hypothesis leads to very good results [7, 8, 22].

The semi-kinetic equations can be written as:

$$\partial_t n + \partial_{\boldsymbol{x}}(n\boldsymbol{u}) - \partial_S(Kn) = 0, \tag{12}$$

$$\partial_t(n\boldsymbol{u}) + \partial_{\boldsymbol{x}}(n\boldsymbol{u}\otimes\boldsymbol{u}) - \partial_S(Kn\boldsymbol{u}) - n\frac{\boldsymbol{u}_g - \boldsymbol{u}}{\mathrm{St}} = 0. \tag{13}$$

Notice that here, $\boldsymbol{u}$ is not equal to $\boldsymbol{u}_g$, and the droplets have their own velocity. In the final system of equation, this will be accounted for by an equation on the momentum for the spray particles.

2.2. Size moment equations

In both cases, moment methods will be used for the simulations. Size moments of order 0 to N are then introduced, thus considering the evolution of the total number density of the particles, their mean size, their mean size squared (which can be linked to the dispersion in size of the NDF), etc... This moments on the non dimensional interval $[0,1]$ are defined as follows:

$$m_k(t,\boldsymbol{x}) = \int_0^1 S^k n(t,\boldsymbol{x},S)\,\mathrm{d}S. \tag{14}$$

For inertial particles, as the moments are advected with their own velocity and not with the gas velocity, an additional equation is needed. Since an accurate description of the particle dynamics conditioned on size is not beyond the scope of the paper, this phenomenon will be described, here, by only one averaged velocity. In fact, the velocity of the particles $\boldsymbol{u}$ is assumed not to depend on particle size. When a size discretization is used, as for multi-fluid methods [25], this assumption is done in each size interval. Here, a discretization can still be done, but the interest of the method comes from the possibility to reduce the number of size intervals (till eventually the case of one single interval) by a better description of each interval through a higher number of moments. The assumption of a "constant" velocity can then appear unjustified. But, as it will be shown in the Result section, the better description of the granulometry through the use of several moments allows to have a good description of the spray dynamic thanks to an improvement of the approximation of the drag force.

From Eq. (8) and system (12,13), the systems on the moments are written:

$$\text{Aerosols}\quad \begin{cases} \partial_t(m_0) + \partial_{\boldsymbol{x}}(m_0\boldsymbol{u}_g) &= \partial_{\boldsymbol{x}}(\boldsymbol{D}\partial_{\boldsymbol{x}}m_0) - Kn(S=0), \\ \partial_t(m_1) + \partial_{\boldsymbol{x}}(m_1\boldsymbol{u}_g) &= \partial_{\boldsymbol{x}}(\boldsymbol{D}\partial_{\boldsymbol{x}}m_1) - Km_0, \\ \partial_t(m_2) + \partial_{\boldsymbol{x}}(m_2\boldsymbol{u}_g) &= \partial_{\boldsymbol{x}}(\boldsymbol{D}\partial_{\boldsymbol{x}}m_2) - 2Km_1, \\ \qquad\qquad \vdots & \\ \partial_t(m_N) + \partial_{\boldsymbol{x}}(m_N\boldsymbol{u}_g) &= \partial_{\boldsymbol{x}}(\boldsymbol{D}\partial_{\boldsymbol{x}}m_N) - NKm_{N-1}, \end{cases} \tag{15}$$

$$\text{Spray}\quad \begin{cases} \partial_t(m_0) + \partial_{\boldsymbol{x}}(m_0\boldsymbol{u}) &= -Kn(S=0), \\ \partial_t(m_1) + \partial_{\boldsymbol{x}}(m_1\boldsymbol{u}) &= -Km_0, \\ \partial_t(m_2) + \partial_{\boldsymbol{x}}(m_2\boldsymbol{u}) &= -2Km_1, \\ \qquad\qquad \vdots & \\ \partial_t(m_N) + \partial_{\boldsymbol{x}}(m_N\boldsymbol{u}) &= -NKm_{N-1}, \\ \partial_t(m_1\boldsymbol{u}) + \partial_{\boldsymbol{x}}(m_1\boldsymbol{u}\otimes\boldsymbol{u}) &= \boldsymbol{T} - Km_0\boldsymbol{u}. \end{cases} \tag{16}$$

The quantity $\boldsymbol{T}$ represents the drag term. It writes $\boldsymbol{T}(t,\boldsymbol{x}) = \int_0^1 Sn(t,\boldsymbol{x},S)\frac{\boldsymbol{u}_g(t,\boldsymbol{x})-\boldsymbol{u}(t,\boldsymbol{x})}{\mathrm{St}}\,\mathrm{d}S$ in the Stokes regime considered here (let us however notice that introducing a more complex drag force does not bring any difficulties). The Stokes number being proportional to the droplet surface, let us denote θ the proportionality coefficient: $\mathrm{St} = \theta S$. The drag force is then written:

$$\boldsymbol{T}(t,\boldsymbol{x}) = \frac{m_0}{\theta}(\boldsymbol{u}_g(t,\boldsymbol{x}) - \boldsymbol{u}(t,\boldsymbol{x})). \tag{17}$$

Let us remark that, if the last equation of (16) had been written on $m_0\boldsymbol{u}$, then the drag term would not have been integrable (the NDF n has generally a non zero value at $S=0$ [30]).

Since our objective is to show a robust and accurate scheme able to transport a moment vector and for the sake of simplicity, the evaporation coefficient K as well as the diffusion operator $\boldsymbol{D}$ for aerosol have been assumed independent of the particle size. We nevertheless remark that these assumptions do not bring any loss of generality. Indeed, in the context of an operator splitting algorithm [38], each operator can be solved separately. Usual numerical schemes can then be used for the diffusion. Concerning the evaporation, the resolution of the corresponding system will be detailed in section 4 with an algorithm developed in [30] and which had been generalized to an arbitrary evaporation law in the same paper. This algorithm allows then a robust resolution of the evaporation part in all cases, through a modeling of the unclosed term $-Kn(S=0)$ (the disappearance flux of droplets through evaporation) and an adapted numerical scheme.

Let us then focus to convection of the moments. An algorithm is here designed for the resolution of the following systems:

$$\text{Aerosols}\quad \begin{cases} \partial_t(m_0) + \partial_{\boldsymbol{x}}(m_0\boldsymbol{u}_g) = 0, \\ \partial_t(m_1) + \partial_{\boldsymbol{x}}(m_1\boldsymbol{u}_g) = 0, \\ \partial_t(m_2) + \partial_{\boldsymbol{x}}(m_2\boldsymbol{u}_g) = 0, \\ \qquad\vdots \\ \partial_t(m_N) + \partial_{\boldsymbol{x}}(m_N\boldsymbol{u}_g) = 0, \end{cases} \qquad \text{Spray}\quad \begin{cases} \partial_t(m_0) + \partial_{\boldsymbol{x}}(m_0\boldsymbol{u}) = 0, \\ \partial_t(m_1) + \partial_{\boldsymbol{x}}(m_1\boldsymbol{u}) = 0, \\ \partial_t(m_2) + \partial_{\boldsymbol{x}}(m_2\boldsymbol{u}) = 0, \\ \qquad\vdots \\ \partial_t(m_N) + \partial_{\boldsymbol{x}}(m_N\boldsymbol{u}) = 0, \\ \partial_t(m_1\boldsymbol{u}) + \partial_{\boldsymbol{x}}(m_1\boldsymbol{u}\otimes\boldsymbol{u}) = 0. \end{cases} \tag{18}$$

However, before designing such algorithm, some key properties of the moment space and of the system have to be recalled. This is the subject of the next two sections.

2.3. Moment space and canonical moments

The major issue of the numerical scheme developed here is to keep the integrity of the moment sequence $(m_0, \ldots, m_N)^t$. Indeed, Wright [41] showed that independent transport of moments with algorithms of order greater than one in space, can result in the generation of invalid moment sets. That means that there is no distribution function $n(t, \boldsymbol{x}, S)$ which can be reconstructed from the moment sequence such as $\int_0^1 S^k n(t, \boldsymbol{x}, S)\, dS = m_k(t, \boldsymbol{x})$.

So, let us first define the moment space. If $\mathcal{P}$ denotes the set of all probability measures on the Borel sets of the interval $[0, 1]$, then the Nth-moment space $\widetilde{\boldsymbol{\mathcal{M}}}_N$ on the interval $[0, 1]$ denotes the following set of moment vector of dimension N, $\widetilde{\boldsymbol{\mathcal{M}}}_N \subset [0, 1]^N$:

$$\widetilde{\boldsymbol{\mathcal{M}}}_N = \{\boldsymbol{c}_n(\mu) | \mu \in \mathcal{P}\}, \quad \mathbf{c}_N(\mu) = (c_1(\mu), \ldots, c_N(\mu))^t, \quad c_k(\mu) = \int_0^1 x^k \, d\mu(x).$$

Since we consider probability measures, we always have $c_0 = 1$. In our case, we are dealing with number density functions, so normalized moments has to be defined: for any non zero moment vector $\mathcal{M} = (m_0, m_1, \ldots, m_N)^t \in \mathbf{R}^{N+1}$, m_0 being the particle number density, the normalized moments are defined as follows:

$$c_k = \frac{m_k}{m_0}. \tag{19}$$

The vector $\boldsymbol{c}_n = (c_1, \ldots, c_n)^t$ is the vector of normalized moments of the distribution function. Let us then denotes $\boldsymbol{\mathcal{M}}_N$ the Nth-moment space of such moment vectors $\mathcal{M}$. Its complex geometry makes it difficult to preserve the moment space. Its only intuitive characteristic is that it is a convex space. In order to study some useful properties of the moment space, we will take benefit from some quantities derived from the moments: the Hankel determinants and the canonical moments [10].

A first useful tools are the Hankel determinants, defined by:

$$\underline{H}_{2m+d} = \begin{vmatrix} c_d & \ldots & c_{m+d} \\ \vdots & & \vdots \\ c_{m+d} & \ldots & c_{2m+d} \end{vmatrix}, \qquad \overline{H}_{2m+d} = \begin{vmatrix} c_{1-d} - c_{2-d} & \ldots & c_m - c_{m+1} \\ \vdots & \vdots & \vdots \\ c_m - c_{m+1} & \ldots & c_{2m-1+d} - c_{2m+d} \end{vmatrix}, \tag{20}$$

with $d = 0, 1$; $m \geq 0$, $\underline{H}_{-1} = \overline{H}_{-1} = \underline{H}_0 = \overline{H}_0 = 1$. Necessary and sufficient conditions for a moment vector $\mathcal{M} = (m_0, m_1, \ldots, m_N)$ to be in the moment space $\boldsymbol{\mathcal{M}}_N$ (i.e. for the existence of a necessarily non unique NDF $n(t, \boldsymbol{x}, S)$) are non negative Hankel determinants $\underline{H}_i$ and $\overline{H}_i$ defined from the corresponding normalized moment, for $i = 1, \ldots, N$ [10]. Moreover, at least one of the Hankel determinant is zero for a moment vector lying on the border of the moment space. Checking if a $N + 1$ component vector belongs to the moment space is quite tedious when $N \geq 2$ because of the complex geometry of the moment space. However, the Hankel determinants provide algebraic relations to quickly determine if a vector belongs to the moment space. Moreover they enable to derive quantities called canonical moments, linked with a one-to-one mapping to the moment space. The canonical moment space has the very convenient property of fully lying in the set $]0, 1[^k$, and not in a subset of it. Therefore, in order to check if the moment space is preserved, it is more practical to work with the canonical moments.

Let us introduce the set $P(\boldsymbol{c}_{k-1})$ of all probability measures on $[0, 1]$ whose moments of order up to $k - 1$ are c_j. Dette and Studden [10] have given the definition of the canonical moments of order k $(k \geq 1)$:

$$p_k = \frac{c_k - c_k^-(\boldsymbol{c}_{k-1})}{c_k^+(\boldsymbol{c}_{k-1}) - c_k^-(\boldsymbol{c}_{k-1})}, \tag{21}$$

with

$$c_k^+(\boldsymbol{c}_{k-1}) = \max_{\mu \in P(\boldsymbol{c}_{k-1})} c_k(\mu), \qquad c_k^-(\boldsymbol{c}_{k-1}) = \min_{\mu \in P(\boldsymbol{c}_{k-1})} c_k(\mu), \tag{22}$$

$c_k(\mu)$ being the moment of order k of the probability measure μ. The quantities $c_k^+(\boldsymbol{c}_{k-1})$ and $c_k^-(\boldsymbol{c}_{k-1})$ are respectively the upper and lower boundary of the admissible interval for the moment c_k of order k, the lower order moments being known. If $c_k(\mu) = c_k^+(\boldsymbol{c}_{k-1})$ or $c_k(\mu) = c_k^-(\boldsymbol{c}_{k-1})$ for $\mu \in P(\boldsymbol{c}_{k-1})$, or equivalently if $p_k = 0$ or $p_k = 1$, the measure μ is a sum of Dirac distributions and the vector $\boldsymbol{c}_k$ belongs to the boundary of the moment space.

The $c_k^+ - c_k^-$ and canonical moments are expressed from the Hankel determinants in [10], for $k \geq 1$:

$$c_k^+ - c_k^- = \frac{\underline{H}_{k-1}\overline{H}_{k-1}}{\underline{H}_{k-2}\overline{H}_{k-2}}, \qquad p_k = \frac{\underline{H}_k\overline{H}_{k-2}}{\underline{H}_{k-1}\overline{H}_{k-1}}. \tag{23}$$

But practically, the canonical moments are recursively determined from the lower order ones. The expressions of the first three canonical moments are:

$$p_1 = c_1, \qquad p_2 = \frac{c_2 - c_1^2}{c_1(1-c_1)}, \qquad p_3 = \frac{(1-c_1)(c_1c_3 - c_2^2)}{(c_2 - c_1^2)(c_1 - c_2)}. \tag{24}$$

The canonical moments have two major properties which make them attractive to work with. First, according to the definition (21), and as it as already been stated, each canonical moment independently lies in the interval $]0,1[$ for a moment vector in the interior of the moment space. It is thus straightforward to figure out if the associated moment vector belongs to the moment space, and if a distribution function can be reconstructed. Secondly, the canonical moments remain invariant under linear transformation of the distribution, i.e for all $k \geq 1$, $p_k(f) = p_k(f_{S_{min}S_{max}})$, where $f_{S_{min}S_{max}}$ denotes the distribution induced by the linear transformation $S = S_{min} + (S_{max} - S_{min})x$ of $[0,1]$ onto $[S_{min}, S_{max}]$ (we refer to [10] for the proof). That is the reason why we can work on the size interval $[0,1]$ without loss of generality.

In addition to the two previous properties, another property given from systems (18) will be very useful when designing the numerical scheme.

Proposition 1. *Let $\boldsymbol{u}(t,\boldsymbol{x})$ be a C^1 function. If the moment vector $(m_0, m_1, \ldots, m_N)$ is a C^1 function of t and $\boldsymbol{x}$ belonging to the interior of the moment space and such that*

$$\begin{cases} \partial_t(m_0) + \partial_{\boldsymbol{x}}(m_0\boldsymbol{u}) = 0, \\ \partial_t(m_1) + \partial_{\boldsymbol{x}}(m_1\boldsymbol{u}) = 0, \\ \partial_t(m_2) + \partial_{\boldsymbol{x}}(m_2\boldsymbol{u}) = 0, \\ \qquad\vdots \\ \partial_t(m_N) + \partial_{\boldsymbol{x}}(m_N\boldsymbol{u}) = 0, \end{cases} \tag{25}$$

then the corresponding canonical moments are transported quantities, which means that they verify the transport equation: $\partial_t p_k + \boldsymbol{u}\partial_{\boldsymbol{x}} p_k = 0$.

Proof. – According to Eq. (23), p_k is a rational fraction of the moments c_k. Moreover, since the moment vector is in the interior of the moment space, the denominator can never be equal to zero. Therefore, $p_k(c_k)$ is differentiable relative to each $c_{j,j\leq k}$. Thus we have the relation:

$$\partial_t p_k + \boldsymbol{u}\,\partial_x p_k = \sum_{j\leq k} \partial_{c_j} p_k \left[\partial_t c_j + \boldsymbol{u}\,\partial_x c_j\right]. \tag{26}$$

But since the c_j are transported quantities, we have $\partial_t p_k + \boldsymbol{u}\partial_x p_k = 0$. □

2.4. Pressureless gas dynamics

Let us remark that the system (18) for the spray contains the pressureless gas dynamics system which has been studied by several authors [1, 3]. Indeed, this system can be written:

$$\partial_t U + \partial_{\boldsymbol{x}} F(U) = 0, \qquad \mathbf{A}(U) = \partial_U F(U), \tag{27}$$

where

$$U = (m_0, \ldots, m_N, m_1u)^t, \qquad F = (m_0u, m_1u, \ldots, m_1u^2), \tag{28}$$

In the pressureless gas system, the Jacobian matrix of the flux $\mathbf{A}$ is a Jordan block, the system is weakly hyperbolic. A main feature of this weakly hyperbolic system is the development of singularities for the conserved quantities called δ-shocks, and the emergence of the vacuum state, even when the initial

distribution is regular. Such a system can be seen as a particular case of a more general class of systems [4] which will allow to capture droplet trajectory crossing such as in [14, 22].

The key issue is thus to design a robust numerical scheme with second order in time and space for the advection of the moments satisfying the realizability condition in both the case of aerosols as well as in the case of sprays where singularity formation can occur. As in many cases, the construction of the discretization will rely on specific properties of the continuous system of partial differential equations we have derived so far. The following section exposes the characteristics of the scheme preserving the moment space, and capturing the singularities introduced by the pressureless gas dynamics.

3. A new finite volume kinetic numerical scheme preserving the moment space

In this section, we present the numerical scheme used to discretize system (18) in the case of an aerosol, and its extension to treat the case of a spray. Because of the conservative form of system (18), the finite-volume method [26] is a natural candidate for its discretization. Moreover, since the computations we present are enforced in a cartesian mesh, we use a dimensional splitting algorithm explained by Strang [38], preserving the second order in time of the scheme and also its mathematical properties. Thus, for example in a 2D framework, to solve the system on a time step Δt, the transport in the first direction is solved for $\Delta t/2$ then the transport in the second direction is solved for Δt and finally, the transport in the first direction is solved for $\Delta t/2$. An alternated Lie splitting (equivalent to a Strang splitting on 2 time steps) can also be used with the advantage of using the 1D transport algorithm with the same time step in each direction [7]. So, without loss of generality, the scheme is then presented in a one dimensional framework, with the addition of the transport equation of a passive scalar corresponding to an eventual velocity component in another direction.

Usually, high order finite volume methods use some non-constant reconstructions of the variables to evaluate the fluxes between the cells. But, the properties of the scheme are related to the expression of the fluxes. Let us recall that two difficulties have to be overcome. The first one concerns the way to do the spatial reconstruction of the moments in order to keep the integrity of the moment set. It has been seen that for a high order in space scheme, an independent reconstruction of each moment does not insure that the moment space is preserved at any spatial point [41, 31]. This will not inevitably lead to instabilities in the convective transport algorithm, even if it can, but some physical information about the size distribution is lost and it results in a performance reduction in terms of computational cost since such situations have to be detected in order to correct them. Once we have designed an algorithm which is able to provide the previous realizability property at any spatial point of the reconstructed moments, a second difficulty concerns the computation of the fluxes from the reconstructed quantities. If an approximate time solver is used (Explicit Euler, Runge-Kutta), the fluxes computation will introduce troncature errors for non constant reconstructions, and the preservation of the moment space would not be guaranteed any more. In order to meet this condition, we design a kinetic-based numerical scheme using the ideas developed by Bouchut [2]. The time solver is based on an exact resolution of the PDE in time which relies on a micro-macro equivalence property, leading to the fact that the fluxes introduce no troncature error with respect to the spatial reconstruction. An exact computation of the fluxes is obtained using the fact that the equations on moments can be derived from the kinetic equivalent equation.

3.1. General form of the kinetic schemes

In a similar manner as in [2], a kinetic scheme is developed, based on the equivalence between the "macroscopic" system and a kinetic equation. The "macroscopic" equation on the size distribution $n(t, x, S)$ is:

$$\partial_t n + \partial_x(nu) = 0, \tag{29}$$

where u is the gas velocity for aerosols and the particle velocity for the spray in the direction we are dealing with. A passive scalar v can also be considered, representing an eventual other direction in the framework of dimensional splitting for a 2D or 3D computation. Both these variables are then a solution of:

$$\partial_t(nu) + \partial_x(nu^2) = 0, \tag{30}$$

$$\partial_t(nv) + \partial_x(nuv) = 0. \tag{31}$$

This "macroscopic" system is equivalent to the kinetic equation on $f(t,x,\xi,\zeta,S)$:

$$\partial_t f + \partial_x(\xi f) = 0, \tag{32}$$

with $f(t,x,\xi,\zeta,S) = n(t,x,S)\delta(\xi - u(t,x))\delta(\zeta - v(t,x))$. This kinetic equation has the exact solution $f(t,x,\xi,\zeta,S) = f(0,x-\xi t,\xi,\zeta,S)$. The strategy to develop the scheme is then the same one as in [2], with the difference that here, the "macroscopic" system of interest (18) is not directly (29) or (29, 30) but a system induced by taking the size moments of these equations.

In order to obtain discrete values over a mesh of constant size Δx, one defines the averages $m^n_{k,j}$, u^n_j and v^n_j for inertial particles, with the usual definitions:

$$m^n_{k,j} = \frac{1}{\Delta x}\int_{x_{j-1/2}}^{x_{j+1/2}} m_k(t_n,x)\,\mathrm{d}x, \qquad k = 0,\dots,N, \tag{33}$$

$$\boldsymbol{q}^n_j = m^n_{1,j}\begin{pmatrix} u^n_j \\ v^n_j \end{pmatrix} = \frac{1}{\Delta x}\int_{x_{j-1/2}}^{x_{j+1/2}} m_1(t_n,x)\begin{pmatrix} u(t_n,x) \\ v(t_n,x)\end{pmatrix}\mathrm{d}x, \tag{34}$$

Let us denote $\mathcal{M}_N = (m_0,\dots,m_N)^t$ the vector of moments. The discretized equations are obtained in a conservative form by integrating Eq. (32) multiplied by $(1,S,\dots,S^N,\xi)^t$ over $(t,x,\xi,S) \in (t_n,t_{n+1})\times(x_{j-1/2},x_{j+1/2})\times\mathbb{R}\times(0,1)$:

$$\begin{aligned} \mathcal{M}^{n+1}_{N,j} &= \mathcal{M}^n_{N,j} - \frac{\Delta t}{\Delta x}(\boldsymbol{F}_{j+1/2} - \boldsymbol{F}_{j-1/2}), \\ \boldsymbol{q}^{n+1}_j &= \boldsymbol{q}^n_j - \frac{\Delta t}{\Delta x}(\boldsymbol{G}_{j+1/2} - \boldsymbol{G}_{j-1/2}), \end{aligned} \tag{35}$$

where the fluxes for the size moments $\boldsymbol{F}_{j+1/2}$ can be decomposed in $\boldsymbol{F}_{j+1/2} = \boldsymbol{F}^+_{j+1/2} + \boldsymbol{F}^-_{j+1/2}$ with:

$$\boldsymbol{F}^\pm_{j+1/2} = \frac{1}{\Delta t}\int_{t_n}^{t_{n+1}}\int_{\pm\xi\geq 0}\int_0^1\int_{\mathbf{R}}\begin{pmatrix} 1 \\ S \\ \vdots \\ S^N\end{pmatrix}\xi\, f(t,x_{j+1/2},\xi,\zeta,S)\,\mathrm{d}\zeta\mathrm{d}S\mathrm{d}\xi\mathrm{d}t, \tag{36}$$

and in the same way, the flux for the momentum in the case of inertial particles is $\boldsymbol{G}_{j+1/2} = \boldsymbol{G}^+_{j+1/2} + \boldsymbol{G}^-_{j+1/2}$ with:

$$\boldsymbol{G}^\pm_{j+1/2} = \frac{1}{\Delta t}\int_{t_n}^{t_{n+1}}\int_{\pm\xi\geq 0}\int_0^1\int_{\mathbf{R}} S\begin{pmatrix}\xi \\ \zeta\end{pmatrix}\xi f(t,x_{j+1/2},\xi,\zeta,S)\,\mathrm{d}\zeta\mathrm{d}S\mathrm{d}\xi\mathrm{d}t. \tag{37}$$

To evaluate the fluxes, the exact solution of the kinetic scheme is used:

$$\begin{aligned}\begin{pmatrix}\boldsymbol{F}^\pm_{j+1/2} \\ \boldsymbol{G}^\pm_{j+1/2}\end{pmatrix} &= \frac{1}{\Delta t}\int_0^{\Delta t}\int_{\pm\xi\geq 0}\int_0^1\begin{pmatrix} 1 \\ S \\ \vdots \\ S^N \\ S\,\xi \\ S\,v(t_n,x_{j+1/2}-\xi t)\end{pmatrix}\xi\, n(t_n,x_{j+1/2}-\xi t,S)\delta(\xi - u(t_n,x_{j+1/2}-\xi t))\,\mathrm{d}S\mathrm{d}\xi\mathrm{d}t \\ &= \frac{1}{\Delta t}\int_0^{\Delta t}\int_{\pm\xi\geq 0}\begin{pmatrix} m_0(t_n,x_{j+1/2}-\xi t) \\ m_1(t_n,x_{j+1/2}-\xi t) \\ \vdots \\ m_N(t_n,x_{j+1/2}-\xi t) \\ m_1(t_n,x_{j+1/2}-\xi t)\xi \\ (m_1 v)(t_n,x_{j+1/2}-\xi t)\end{pmatrix}\xi\,\delta(\xi - u(t_n,x_{j+1/2}-\xi t))\,\mathrm{d}\xi\mathrm{d}t.\end{aligned}$$

Let us develop the computation for $(\boldsymbol{F}^+_{j+1/2}, \boldsymbol{G}^+_{j+1/2})$. A change of variable between t and $x = x_{j+1/2} - \xi t$ gives:

$$\begin{pmatrix} \boldsymbol{F}^+_{j+1/2} \\ \boldsymbol{G}^+_{j+1/2} \end{pmatrix} = \frac{1}{\Delta t} \int_{\xi \geq 0} \int_{x_{j+1/2} - \xi \Delta t}^{x_{j+1/2}} \begin{pmatrix} m_0(t_n, x) \\ m_1(t_n, x) \\ \vdots \\ m_N(t_n, x) \\ m_1(t_n, x)\xi \\ (m_1 v)(t_n, x) \end{pmatrix} \delta(\xi - u(t_n, x)) \, \mathrm{d}\xi \mathrm{d}x$$

$$= \frac{1}{\Delta t} \int_{x_{j-1/2}}^{x_{j+1/2}} \begin{pmatrix} m_0(t_n, x) \\ m_1(t_n, x) \\ \vdots \\ m_N(t_n, x) \\ m_1(t_n, x)u(t_n, x) \\ m_1(t_n, x)v(t_n, x) \end{pmatrix} \mathbb{1}_{\{x, x_{j+1/2} - u(t_n, x)\Delta t \leq x \leq x_{j+1/2}\}}(x) \, \mathrm{d}x, \tag{38}$$

the last expression being valid under the CFL condition: $\Delta t \sup_x |u(t_n, x)| \leq \Delta x$. In the same way, the other part of the fluxes are:

$$\begin{pmatrix} \boldsymbol{F}^-_{j+1/2} \\ \boldsymbol{G}^-_{j+1/2} \end{pmatrix} = -\frac{1}{\Delta t} \int_{x_{j-1/2}}^{x_{j+1/2}} \begin{pmatrix} m_0(t_n, x) \\ m_1(t_n, x) \\ \vdots \\ m_N(t_n, x) \\ m_1(t_n, x)u(t_n, x) \\ m_1(t_n, x)v(t_n, x) \end{pmatrix} \mathbb{1}_{\{x, x_{j+1/2} \leq x \leq x_{j+1/2} - u(t_n, x)\Delta t\}}(x) \, \mathrm{d}x. \tag{39}$$

The fluxes are then written with the variables of interest: the moments m_k of the size distribution n. The difficulty now is to reconstruct the moments $m_k(t_n, .)$ from the $m^n_{k,j}$ in such a way that the moment space is preserved. In order to show how this scheme is built in a simple case, we will first compute the convective fluxes in the context of a first order kinetic scheme. But a first order scheme is not satisfactory, as our goal is to design a scheme with very limited diffusion.

3.2. First order kinetic scheme

For a first order kinetic scheme, piecewise constant data are reconstructed:

$$\text{for } \; x_{j-1/2} < x < x_{j+1/2} \qquad \begin{cases} m_k(t_n, x) = m^n_{k,j}, & k = 0, \ldots, N \\ u(t_n, x) = u^n_j \\ v(t_n, x) = v^n_j \end{cases} \tag{40}$$

Under the CFL condition $\Delta t \sup_j |u^n_j| \leq \Delta x$, the expression of the fluxes (38,39) are straightforward:

$$\boldsymbol{F}^+_{j+1/2} = \mathcal{M}^n_{N,j}(u^n_j)_+, \qquad \boldsymbol{G}^+_{j+1/2} = m^n_{1,j} \begin{pmatrix} u^n_j \\ v^n_j \end{pmatrix} (u^n_j)_+, \tag{41}$$

and

$$\boldsymbol{F}^-_{j+1/2} = \mathcal{M}^n_{N,j+1}(u^n_{j+1})_-, \qquad \boldsymbol{G}^-_{j+1/2} = m^n_{1,j+1} \begin{pmatrix} u^n_{j+1} \\ v^n_{j+1} \end{pmatrix} (u^n_{j+1})_-, \tag{42}$$

with the convention $u_+ = \max\{u, 0\}$, $u_- = \min\{u, 0\}$.

With piecewise constant reconstructions, the first order scheme considerably simplifies the reconstruction step as it eludes the problem of preservation of the moment space which arises when non constant

reconstruction are considered. Indeed, this first order scheme can be written:

$$\mathcal{M}_{N,j}^{n+1} = \left(1 - \frac{\Delta t}{\Delta x}|u_j^n|\right)\mathcal{M}_{N,j}^n - \frac{\Delta t}{\Delta x}(u_{j+1}^n)_-\mathcal{M}_{N,j+1}^n + \frac{\Delta t}{\Delta x}(u_{j-1}^n)_+\mathcal{M}_{N,j-1}^n \tag{43}$$

$$= \int_0^1 \begin{pmatrix} 1 \\ S \\ \vdots \\ S^N \end{pmatrix} \left[\left(1 - \frac{\Delta t}{\Delta x}|u_j^n|\right) f_j - \frac{\Delta t}{\Delta x}(u_{j+1}^n)_- f_{j+1} + \frac{\Delta t}{\Delta x}(u_{j-1}^n)_+ f_{j-1}\right](S)\,\mathrm{d}S, \tag{44}$$

where f_j is a distribution function with the moments of order 0 to N given by $\mathcal{M}_{N,j}^n$. Under the CFL condition, the coefficients before each f_j are non negative and then, $\mathcal{M}_{N,j}^{n+1}$ is a moment vector. In the case of spray, the first order scheme also satisfies the maximum principle on the velocity. Other properties, like entropy inequalities or the TVD property on the velocity, can also be proved, see [1].

The first order scheme is easy to design, and robust, but, as it is well known, this scheme brings a lot of numerical diffusion. We thus aim at designing a second order in time and space kinetic scheme with presice time integration of the fluxes at the inferfaces which will lead to a vry low level of numerical diffusion while still preserving the moment space.

3.3. Second order kinetic scheme

For the purpose of a second order scheme, a piecewise linear reconstruction is considered. As in [2], we would like to do that on the droplet number density, m_0 and on transported quantities like the velocity. But this cannot be done directly on the normalized moments, independently, since this would lead to a dead end [41]: considering the complexity of the moment space, such reconstruction can not induced moment vectors inside the moment space for all the points of the cell. However, reconstructing the canonical moments enables to preserve the integrity of the moment set at each point of the cell. Indeed, as they are proven to be transported quantities by system (18), they satisfy a maximum principle. They also have the property, as explained in (2.3), to live in $]0,1[^k$ and not in a subset of it. In the context of this paper, we will restrict ourselves on the case $N = 3$. A greater value for N could be considered without difficulty but would lead to more complex algebra and computational cost without a dramatic improvement of the accuracy of the method.

3.3.1. Reconstruction

The reconstruction writes:

$$\text{for } \; x_{j-1/2} < x < x_{j+1/2} \qquad \left\{\begin{array}{rcl} m_0(x) &=& m_{0,j}^n + D_{m_{0,j}}(x - x_j,) \\ p_1(x) &=& \overline{p_{1,j}} + D_{p_{1,j}}(x - x_j), \\ p_2(x) &=& \overline{p_{2,j}} + D_{p_{2,j}}(x - x_j), \\ p_3(x) &=& \overline{p_{3,j}} + D_{p_{3,j}}(x - x_j), \\ u(x) &=& \overline{u_j} + D_{u_j}(x - x_j), \\ v(x) &=& \overline{v_j} + D_{v_j}(x - x_j), \end{array}\right. \tag{45}$$

where $x_j = (x_{j+1/2} + x_{j-1/2})/2$ is the center of the j^{th} cell and where, to simplify the notation, the t_n dependance of each function is implicit. The quantities with bars are different from the canonical moments $p_{i,j}$ corresponding to the moment vector $\mathcal{M}_{3,j}^n$ and from the mean velocities u_j^n and v_j^n. In order to have the conservation property, they are defined in such a way that (according to (24)):

$$m_{1,j}^n = \frac{1}{\Delta x}\int_{x_{j-1/2}}^{x_{j+1/2}} m_0(x)p_1(x)\,\mathrm{d}x,$$

$$m_{2,j}^n = \frac{1}{\Delta x}\int_{x_{j-1/2}}^{x_{j+1/2}} m_0(x)p_1(x)[(1-p_1)p_2 + p_1](x)\,\mathrm{d}x,$$

$$m_{3,j}^n = \frac{1}{\Delta x}\int_{x_{j-1/2}}^{x_{j+1/2}} m_0(x)p_1(x)\{(1-p_1)(1-p_2)p_2p_3 + [(1-p_1)p_2 + p_1]^2\}(x)\,\mathrm{d}x,$$

$$m_{1,j}^n u_j^n = \frac{1}{\Delta x}\int_{x_{j-1/2}}^{x_{j+1/2}} m_0(x)p_1(x)u(x)\,\mathrm{d}x,$$
$$m_{1,j}^n v_j^n = \frac{1}{\Delta x}\int_{x_{j-1/2}}^{x_{j+1/2}} m_0(x)p_1(x)v(x)\,\mathrm{d}x. \tag{46}$$

For the first canonical moment, it is easy to see that:

$$\overline{p_{1,j}} = \frac{m_{1,j}^n}{m_{0,j}^n} - \frac{D_{p_{1,j}}D_{m_{0,j}}}{m_{0,j}^n}\frac{\Delta x^2}{12}, \tag{47}$$

When considering higher order canonical moments $\overline{p_2}$ and $\overline{p_3}$ and the velocity $\overline{u_j}$, their expression are more difficult to figure out, since high order polynomials must be integrated, (up to order 4 for $\overline{p_2}$ and $\overline{u_j}$, and 6 for $\overline{p_3}$). Their expression are written:

$$\overline{u_j} = u_j^n + b_{u,j}D_{u_j}, \qquad \overline{v_j} = v_j^n + b_{v,j}D_{v_j}, \qquad \overline{p_{2,j}} = a_{2,j} + b_{2,j}D_{p_{2,j}}, \qquad \overline{p_{3,j}} = a_{3,j} + b_{3,j}D_{p_{3,j}}, \tag{48}$$

where $b_{u,j} = b_{v,j}$ is independent of D_{u_j} and D_{v_j}, $a_{2,j}$ and $b_{2,j}$ are independent of $D_{p_{2,j}}$ and $a_{3,j}$ and $b_{3,j}$ are independent of $D_{p_{3,j}}$. They are given by:

$$b_{u,j}\int_{x_{j-1/2}}^{x_{j+1/2}} m_0(x)p_1(x)\,\mathrm{d}x = -\int_{x_{j-1/2}}^{x_{j+1/2}} m_0(x)p_1(x)(x-x_j)\,\mathrm{d}x, \tag{49}$$

$$a_{2,j}\int_{x_{j-1/2}}^{x_{j+1/2}} \{m_0p_1[1-p_1]\}(x)\,\mathrm{d}x = m_{2,j}^n\Delta x - \int_{x_{j-1/2}}^{x_{j+1/2}} m_0(x)p_1^2(x)\,\mathrm{d}x, \tag{50}$$
$$b_{2,j}\int_{x_{j-1/2}}^{x_{j+1/2}} \{m_0p_1[1-p_1]\}(x)\,\mathrm{d}x = -\int_{x_{j-1/2}}^{x_{j+1/2}} \{m_0p_1[1-p_1]\}(x)(x-x_j)\,\mathrm{d}x, \tag{51}$$

and

$$a_{3,j}\int_{x_{j-1/2}}^{x_{j+1/2}} \{m_0p_1(1-p_1)(1-p_2)p_2\}(x)\,\mathrm{d}x = m_{3,j}^n\Delta x - \int_{x_{j-1/2}}^{x_{j+1/2}} \{m_0p_1[(1-p_1)p_2+p_1]^2\}(x)\,\mathrm{d}x, \tag{52}$$
$$b_{3,j}\int_{x_{j-1/2}}^{x_{j+1/2}} \{m_0p_1(1-p_1)(1-p_2)p_2\}(x)\,\mathrm{d}x = -\int_{x_{j-1/2}}^{x_{j+1/2}} \{m_0p_1(1-p_1)(1-p_2)p_2\}(x)(x-x_j)\,\mathrm{d}x. \tag{53}$$
$$\tag{54}$$

The calculation of these coefficients is achieved using Maple (Maplesoft, a division of Waterloo Maple, Inc 2007) and are directly exported as Fortran 90 subroutines. Their expression is quite heavy, but, as it is just an algebraic relation, the corresponding CPU cost is low. In a general way, let us write $\overline{p_{i,j}} = a_{i,j} + b_{i,j}D_{p_{i,j}}$ for $i = 1, 2, 3$.

3.3.2. Slope limitation

Once the conservativity of the scheme is ensured, the slopes are determined using limiters in order to satisfy maximum principles for the transported quantities and positivity for the number density. First, for the positivity of number density, the slope $D_{m_{0,j}}$ must verify;

$$|D_{m_{0,j}}\frac{\Delta x}{2}| < m_{0,j}^n. \tag{55}$$

To guarantee the maximum principle on the canonical moments ($i = 1, 2, 3$):

$$r_{ij} \le p_i(x) \le R_{ij}, \qquad x \in (x_{j-1/2}, x_{j+1/2}),$$

where $r_{ij} = \min(p_{i,j-1}, p_{i,j}, p_{i,j+1})$ and $R_{ij} = \max(p_{i,j-1}, p_{i,j}, p_{i,j+1})$, we must have:

$$\begin{cases} r_{i,j} \leq a_{i,j} + b_{i,j} D_{p_{i,j}} + \dfrac{\Delta x}{2} D_{p_{i,j}} \leq R_{i,j}, \\ \\ r_{i,j} \leq a_{i,j} + b_{i,j} D_{p_{i,j}} - \dfrac{\Delta x}{2} D_{p_{i,j}} \leq R_{i,j}. \end{cases} \tag{56}$$

From (47), (51) and (53), it is easy to see that $|b_{i,j}| < \Delta x/2$ for all $i = 1, 2, 3$. The slopes must then verify:

$$\begin{cases} D_{p_{i,j}} \leq min\left(\dfrac{R_{i,j} - a_{i,j}}{b_{i,j} + \Delta x/2}, \dfrac{a_{i,j} - r_{i,j}}{\Delta x/2 - b_{i,j}} \right), \\ \\ D_{p_{i,j}} \geq min\left(\dfrac{r_{i,j} - a_{i,j}}{b_{i,j} + \Delta x/2}, \dfrac{a_{i,j} - R_{i,j}}{\Delta x/2 - b_{i,j}} \right). \end{cases}$$

In practice, we use the following slope limiter to satisfy all the conditions:

$$\begin{aligned} D_{m_{0,j}} &= \frac{1}{2}(sgn(m^n_{0,j+1} - m^n_{0,j}) + sgn(m^n_{0,j} - m^n_{0,j-1})) \times \min\left(\frac{|m^n_{0,j+1} - m^n_{0,j}|}{\Delta x}, \frac{|m^n_{0,j} - m^n_{0,j-1}|}{\Delta x}, \frac{2m^n_{0,j}}{\Delta x} \right), \\ D_{p_{i,j}} &= \frac{1}{2}(sgn(p_{i,j+1} - p_{i,j}) + sgn(p_{i,j} - p_{i,j-1})) \times \min\left(\frac{|p_{i,j+1} - a_{i,j}|}{\Delta x + 2b_{i,j}}, \frac{|a_{i,j} - p_{i,j-1}|}{\Delta x - 2b_{i,j}} \right). \end{aligned} \tag{57}$$

The velocity can be treated like p_2, with an additional condition linked to the CFL limitation:

$$\begin{aligned} D_{u_j} &= \frac{1}{2}(sgn(u^n_{j+1} - u^n_j) + sgn(u^n_j - u^n_{j-1})) \times \min\left(\frac{|u^n_{j+1} - u^n_j|}{\Delta x + 2b_{u,j}}, \frac{|u^n_j - u^n_{j-1}|}{\Delta x - 2b_{u,j}}, \frac{1}{\Delta t} \right), \\ D_{v_j} &= \frac{1}{2}(sgn(v^n_{j+1} - v^n_j) + sgn(v^n_j - v^n_{j-1})) \times \min\left(\frac{|v^n_{j+1} - v^n_j|}{\Delta x + 2b_{v,j}}, \frac{|v^n_j - v^n_{j-1}|}{\Delta x - 2b_{v,j}}, \frac{1}{\Delta t} \right). \end{aligned}$$

Let us remark that for aerosols, a simpler reconstruction can be used for the velocity u which is the gas velocity, since no moment has to be conserved. We can then take $\overline{u_j} = u^n_j$ and D_{u_j} can be a classical slope limiter.

3.3.3. Fluxes computation

Then we can proceed with the evaluation of the fluxes:

$$\begin{pmatrix} \boldsymbol{F}^+_{j+1/2} \\ \boldsymbol{G}^+_{j+1/2} \end{pmatrix} = \frac{1}{\Delta t} \int_{x^L_{j+1/2}}^{x_{j+1/2}} m_0(x) \begin{pmatrix} 1 \\ p_1 \\ p_1[(1-p_1)p_2 + p_1] \\ p_1\{(1-p_1)(1-p_2)p_2p_3 + [(1-p_1)p_2 + p_1]^2\} \\ p_1 u \\ p_1 v \end{pmatrix} (x)\, \mathrm{d}x, \tag{58}$$

where $x^L_{j+1/2}$ is the abscissa of the last droplets reaching $x_{j+1/2}$ at Δt.

$$x^L_{j+1/2} = x_{j+1/2} - \Delta t \frac{(\overline{u}_j + \frac{\Delta x}{2} D_{u_j})_+}{1 + \Delta t D_{u_j}}. \tag{59}$$

Similarly,

$$\begin{pmatrix} \boldsymbol{F}^-_{j+1/2} \\ \boldsymbol{G}^-_{j+1/2} \end{pmatrix} = -\frac{1}{\Delta t} \int_{x_{j+1/2}}^{x^R_{j+1/2}} m_0(x) \begin{pmatrix} 1 \\ p_1 \\ p_1[(1-p_1)p_2 + p_1] \\ p_1\{(1-p_1)(1-p_2)p_2p_3 + [(1-p_1)p_2 + p_1]^2\} \\ p_1 u \\ p_1 v \end{pmatrix} (x)\, \mathrm{d}x, \tag{60}$$

with

$$x^R_{j+1/2} = x_{j+1/2} - \Delta t \frac{(\overline{u_{j+1}} - \frac{\Delta x}{2} D_{u_{j+1}})_-}{1 + \Delta t D_{u_{j+1}}}. \tag{61}$$

The calculation of these fluxes is also achieved using Maple (Maplesoft, a division of Waterloo Maple, Inc 2007) and, once again, we obtain the final Fortran 90 subroutines by exporting the computer algebra results. Their expression is quite heavy, but, as it is just an algebraic relation, the corresponding CPU cost is, once again, quite reasonable.

This kinetic based scheme, using the property of the canonical moments, preserves the moment space directly, without the use of an additional projection algorithm. The need to preserve the realizability condition also comes from the use of dedicated solvers in the size phase space which require access to a distribution function. In particular, our purpose is to evaporate the droplets, which leads us to couple this scheme to the evaporation solver explained in [30]. We summarize its main characteristics in the next section.

4. Evaporation model and associated numerical scheme

As already said, in the context of an operator splitting algorithm, each operator of system (16) is resolved separately. For the evaporation, a set of ODE system (one for each cell of the discretization) is obtained:

$$\begin{cases} \mathrm{d}_t m_0 &= -Kn(S=0), \\ \mathrm{d}_t m_1 &= -Km_0, \\ &\vdots \\ \mathrm{d}_t m_N &= -NKm_{N-1}, \end{cases} \tag{62}$$

the velocity being constant. The underlying kinetic equation reads:

$$\partial_t n - \partial_S (Kn) = 0. \tag{63}$$

A robust and accurate kinetic scheme was developed in [30] for the resolution with a moment method of this purely evaporative case. In particular, this scheme is able to preserve the moment space. Moreover, it has been generalized to an arbitrary evaporation law, depending on the droplet size S and on t (through the dependance on the gas variables) [30]. We summarize herein its main features in the case of a constant evaporation rate.

System (62) has to be closed, since the term $-Kn(S=0)$, representing the disappearing flux of droplets at time t, is a pointwise value of the NDF which has to be related to values of moments in order to provide a closed system. Finding the continuous values of n from the data of its first N moments amounts to solve the finite Hausdorff moment problem [10] for the set in [0,1]. This is done using an Entropy Maximization [32]. Consequently, the value of the NDF appearing in the first equation of system (62) is not genuinely n, but a reconstructed distribution, denoted $f_{ME}(t,S)$.

When it comes to the numerical scheme, plugging system (62) in a ODE like solver leads to serious stability problems. The solution used to avoid these problems is to consider an integrated version in time of the system (62):

$$\exp(K\Delta t\, \mathbf{A})\, \mathcal{M}_N^{n+1} = \mathcal{M}_N^n - \mathbf{\Phi}^-, \tag{64}$$

where

$$\mathcal{M}_N^n = \begin{pmatrix} m_0 \\ \vdots \\ m_N \end{pmatrix}(t_n), \qquad \mathbf{A} = \begin{bmatrix} 0 & & & & 0 \\ 1 & 0 & & & \\ & 2 & \ddots & & \\ & & \ddots & \ddots & \\ 0 & & & N & 0 \end{bmatrix}, \qquad \mathbf{\Phi}^- = \int_0^{K\Delta t} n(t_n,\alpha) \begin{bmatrix} 1 \\ \alpha \\ \vdots \\ \alpha^N \end{bmatrix} \mathrm{d}\alpha, \tag{65}$$

the form of the flux being found using the analytical solution of the kinetic equation (63), in the context of kinetic schemes. This integral form decouples pure transport with no flux from the evolution of the moments through the fluxes.

Thus, the fluxes are computed using the reconstructed distribution $f_{ME}(t_n,.)$ of the distribution $n(t_n,.)$ from its moments $\mathcal{M}_N^n$. For the pure transport part, a last ingredient is introduced: the computation of a quadrature of the moment vector $\mathcal{M}_N$ ($N = 2n_a - 1$ being odd). Indeed, there exist a unique vector of weight $(\omega_i)_{i\leq n_a}$ and a unique vector of abscissas $(\mathcal{S}_i)_{i\leq n_a}$ such that $m_k = \sum_{i=1}^{n_a} \omega_i \mathcal{S}_i^k$ for each $k = 0,\ldots,N$. The following formula shows that this pure transport is only a translation of the abscissas (this is equivalent to a DQMOM approach [15]):

$$\exp(K\Delta t\,\mathbf{A}) \begin{pmatrix} \sum_{i=1}^{n_a} \omega_i(t_n) \\ \sum_{i=1}^{n_a} \omega_i(t_n)\,\mathcal{S}_i(t_n) \\ \vdots \\ \sum_{i=1}^{n_a} \omega_i(t_n)\,\mathcal{S}_i^N(t_n) \end{pmatrix} = \begin{pmatrix} \sum_{i=1}^{n_a} \omega_i(t_n) \\ \sum_{i=1}^{n_a} \omega_i(t_n)(\mathcal{S}_i(t_n) + \Delta t K) \\ \vdots \\ \sum_{i=1}^{n_a} \omega_i(t_n)(\mathcal{S}_i(t_n) + \Delta t K)^N \end{pmatrix}. \tag{66}$$

The resulting algorithm is then [30]:

1. Using the Entropy Maximization, we provide a reconstruction $f_{ME}(t_n,.)$ of the distribution from its moments $\mathcal{M}_N^n$ and flux $\mathbf{\Phi}^-$ is computed from this reconstruction.
2. The weights ω_i and the abscissas $\mathcal{S}_i$ corresponding to the moment vector $\mathcal{M}_N^n - \mathbf{\Phi}^-$ are computed using the QD algorithm [10].
3. The moments $\mathcal{M}_N^{n+1}$ corresponding to the weights ω_i and the abscissas $\mathcal{S}_i - K\Delta t$ are computed.

This algorithm is valid for a CFL-like condition $K\Delta t < 1$.

5. From numerical validation to accuracy and performance assessment

This section is devoted to three representative test-cases, with increasing difficulties, to check the robustness, the accuracy and computational efficiency of the proposed numerical scheme and algorithm. The first one is a one-dimensional case configuration for which an analytical solution exists. It allows to assess quantitatively the accuracy of the method for both aerosol and evaporating spray, as well as its robustness. In a second test-case, a cloud of inertial particles evolves in a two-dimensional Taylor-Green configuration for the gaseous velocity field. This case study allows us to prove the computational efficiency and the good behavior of the scheme. Finally, an injection of a polydisperse spray in an unsteady gaseous flow field constituted of a weakly turbulent free jet is tested. Such a case, while still an academic test-case, is close to more realistic configurations and shows the robustness of the scheme in a more complex environment. We provide a detailed comparison with results given by the multi-fluid model and assess the efficiency of the proposed approach. Let us underline that such a configuration has been introduced in the Ph.D. Thesis of Hicham Meftah [33] at CORIA and that we have compared the Eulerian multi-fluid approach to a reference Lagrangian simulation in [8, 7]. The conclusions of this study was that the fuel mass fraction issued from evaporation was extremely well predicted by the multi-fluid approach, thus making it also a reference solution as far as the present method is concerned.

5.1. Validation by comparison with the analytical solution for 1D transport

Let first simulate the transport at constant velocity of a polydisperse aerosol. The gas velocity is taken as constant and equal to one everywhere and an aerosol is initially present in half of the domain $[0,1]$, the boundary conditions being periodic. Its size distribution has initially a concave shape at $x = 0$ (part of the sinusoid) and a convex one at $x = 0.5$ (decreasing exponential) and evolve continuously between these two points:

$$n(t=0,x,S) \quad = \quad \begin{cases} \lambda(x)\sin(\pi S) + (1-\lambda(x))\exp(-10\,S), & x \leq 0.5, \\ 0, & x > 0.5, \end{cases} \tag{67}$$

where $\lambda(x) = 4(0.5-x)^2$. The first four size moments of this initial distribution are displayed on Fig. 1-left. The constant velocity field is also represented. According to this velocity field, we expect a translation of all the moments at velocity one. That is indeed what we obtain in Fig. 1-right, the numerical simulation being performed in a 200 cells grid with a convective CFL equal to one. The first conclusion, that we can draw from this simple test-case is that only numerical diffusion alters the accuracy of the moment resolution. We must highlight the fact that this is done without an extra projection algorithm, yet yields a high precision.

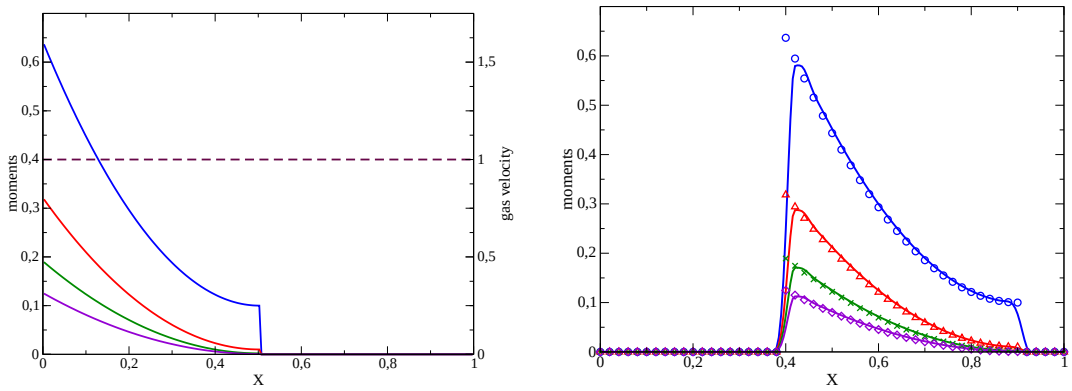

Figure 1: Evolution of aerosol particles calculated with the moment method, in a constant velocity field. (left) Initial condition; the plain curves represent, with decreasing ordering in terms of value, the four first moments from the 0^{th} order (highest) to the 3^{rd} (lowest). The plain curves are scaled by the left Y-axis and the dashed curve representing the velocity field, is scaled by the right Y-axis. (right) Solution at time $t = 0.4$ compared to the analytical solution of the problem represented by marquers.

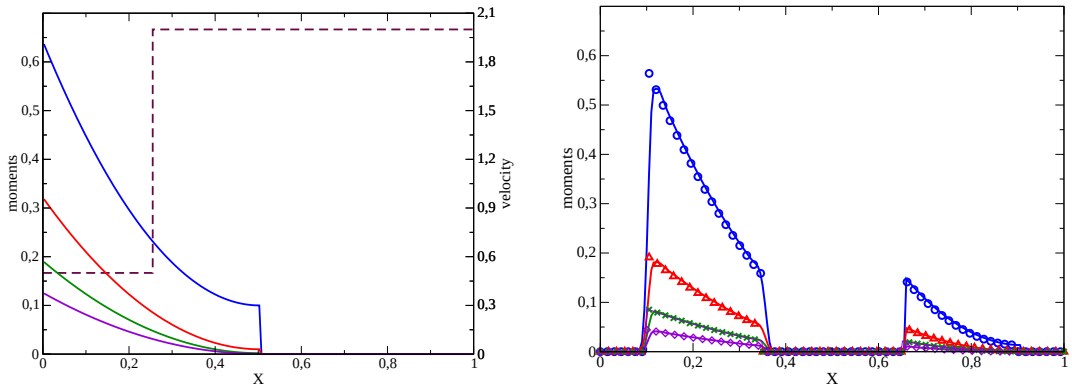

Figure 2: Evolution of a spray in a discontinuous velocity field, calculated with the moment method, compared to the analytical solution of the problem. (left) Initial condition; the plain curves represent, with decreasing ordering in terms of value, the four first moments from the 0^{th} order (highest) to the 3^{rd} (lowest). The plain curves are scaled by the left Y-axis and the dashed curve representing the velocity field, is scaled by the right Y-axis. (right) Solution at $t = 0.2$ compared to the analytical solution of the problem represented by marquers.

In the second test-case, a quantitative comparison with an analytical solution of the transport of an evaporating spray of ballistic droplets is performed. For this problem, we choose the same size distribution as before, but now the particles have their own velocity, initiated by:

$$u(x) \quad = \quad \begin{cases} 0.5, & x \leq 0.25, \\ 2, & x > 0.25. \end{cases} \tag{68}$$

The initial conditions are displayed in Fig. 2-left. As we consider ballistic droplets, the particle dynamics is not influenced by the gas. Besides, the droplets are assumed to be evaporated at rate $K = 1$. The spatial velocity discontinuity makes the droplet cloud spread into two separate clouds with two distinct velocities. This configuration shows the ability of the method to handle the vacuum zone generated by the separation of the clouds. Moreover, because of periodic boundary conditions, the faster cloud will meet the slower one once it has re-entered on the left side. Figure 2-right displays the four analytical size moments, and the size moments given by the calculation at the time $t = 0.2$, performed in a 200 cells grid with a convective CFL equal to one. Figure 3 display the four moments at times $t = 0.4$. We can notice that one, the numerical solution perfectly matches the analytical one, and two, that *a fortiori* the moment space is preserved. The initial distribution breaks into two parts. Vacuum is created at the

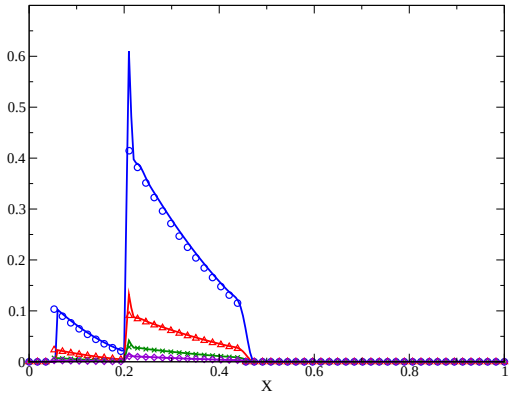

Figure 3: Evolution of a spray in a discontinuous velocity field calculated with the moment method, compared to the analytical solution of the problem. Solution at time $t = 0.4$ compared to the analytical solution of the problem represented by marquers.

initial velocity discontinuity. At t=0.4, the fastest portion catches up the slower one. As we consider a pressureless gas formalism for the particles, nothing prevents the particles from accumulating. However, it must be kept in mind that we do not take collision into account, and the real physical solution would result in a crossing of the clouds, which is represented by the analytical solution. Simulating jet crossing is an issue in Eulerian models and and new methods have been recently designed in the literature and we refer to [14, 4, 22] for references. After the shock has developed, our model is no more valid and the scheme would have been extended to treat this case, in the same way as it was done in orignally in [9, 8] for the multi-fluid model. This is the material of a forthcoming paper. The conclusion of that test-case study reveals that our numerical approach is highly accurate in relation to transport and evaporation and still preserves the realizability condition even in the presence of singularity formation due to pressureless gas dynamics thanks to the design of the proposed kinetic schemes.

5.2. Two dimensional dynamics of a droplet cloud in Taylor-Green vortices

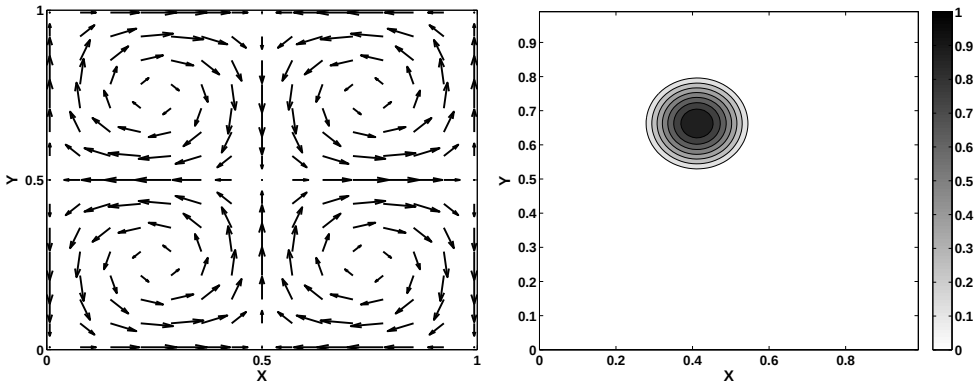

Figure 4: (left) Taylor-Green configuration for the gas vorticity field, (right) Initial condition for the droplets, composed of a motionless cloud. The droplet mass is represented, which is reconstructed from the first four size moments: (m_0, m_1, m_2, m_3)

Let us test our high order moment method in a multi-dimensional configuration with vortices: the 2-D Taylor-Green vortex flow, a steady solution of the inviscid incompressible Euler equations. The gaseous non-dimensional velocity field is then given by $u_{g,x} = \sin(2\,\pi\,x)\,\cos(2\,\pi\,y)$ for its horizontal component and $u_{g,y} = -\cos(2\,\pi\,x)\,\sin(2\,\pi\,y)$ for its vertical one, with $(x, y) \in [0, 1]^2$ and with periodic boundary conditions. The structure of the flow field is presented in Fig. 4-left through the velocity vectors. The

initialization of the spray corresponds to a motionless cloud overlapping two different vortex areas, which will be dragged by the gas. Figure 4-right shows the initial spatial mass distribution provided by a cardinal sinus function. The size distribution of the droplets is initially uniform, with a NDF as well the corresponding mass distribution function represented in Fig. 5.

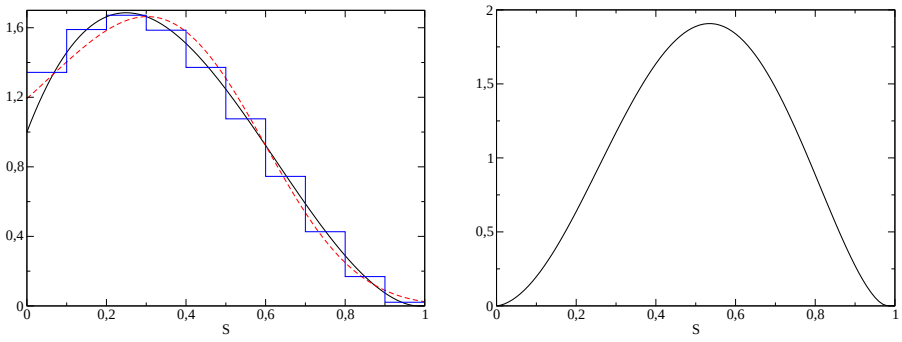

Figure 5: (left) Initial size distribution for the particles (solid line), its reconstruction by the Entropy Maximization from its first 4 moments (dashed line) and initial mass distribution for the multi-fluid method (piece constant function). (right) Corresponding mass distribution.

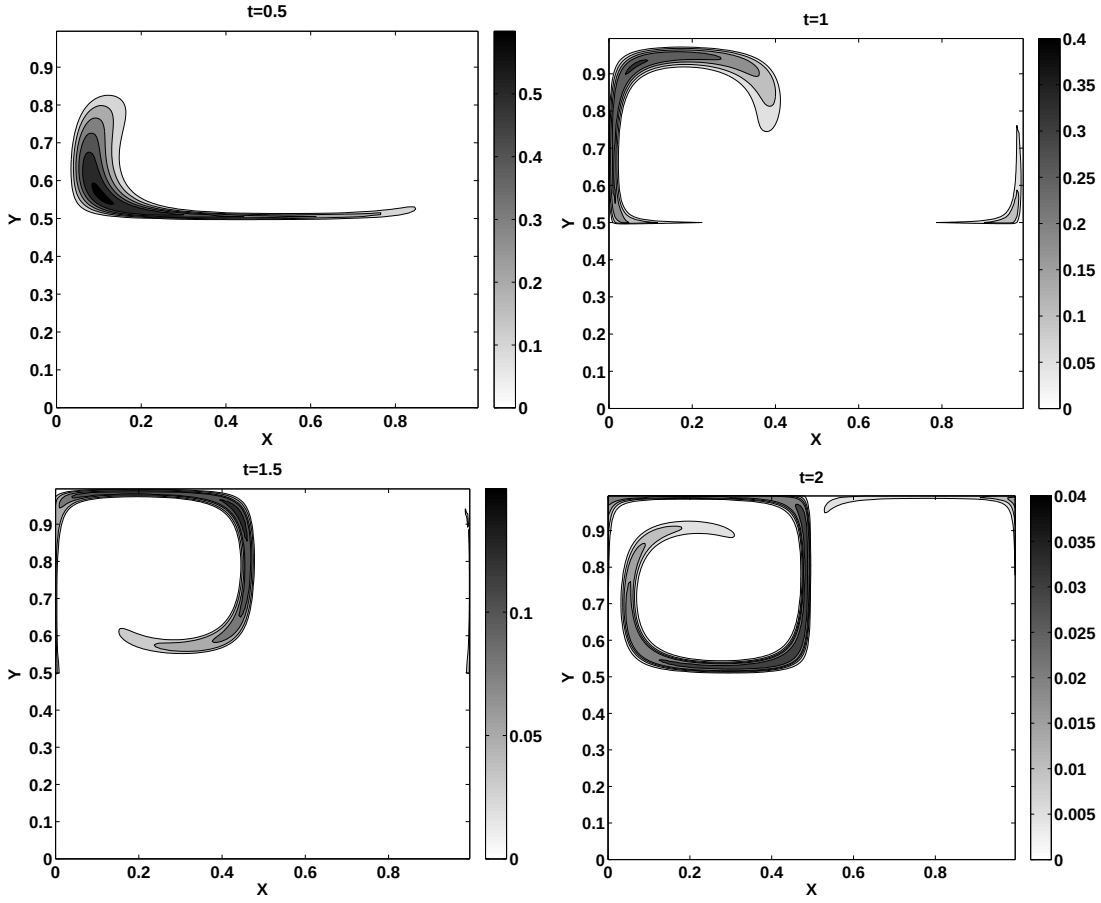

Figure 6: Results for spray dynamics dragged by the gas field made of Taylor-Green vortices, computed with the high order moment method. Droplet mass at time $t = 0.5$ (top-left), $t = 1$ (top-right), $t = 1.5$ (bottom-left), $t = 2$ (bottom-right). The computation is carried out in a 200×200 grid.

Two sets of computations are launched, one for the high order moment method and the other one for the multi-fluid model with ten sections. Both are done till the non dimensional time $t = 2$, corresponding to two eddy turn over times. Moreover, we have chosen a 200×200 grid cell, to ensure that we have a sufficiently detailed description of the field and, as in the earlier cases, the CFL number is equal to one. The results of the multi-fluid model are used as the reference to validate our method. The field compared between the two results is the droplet mass which is naturally solved in the multi-fluid model, whereas it is reconstructed from the four moments (m_0, m_1, m_2, m_3) in the high order moment method, using the reconstruction f_{ME} computed by Entropy Maximization [30].

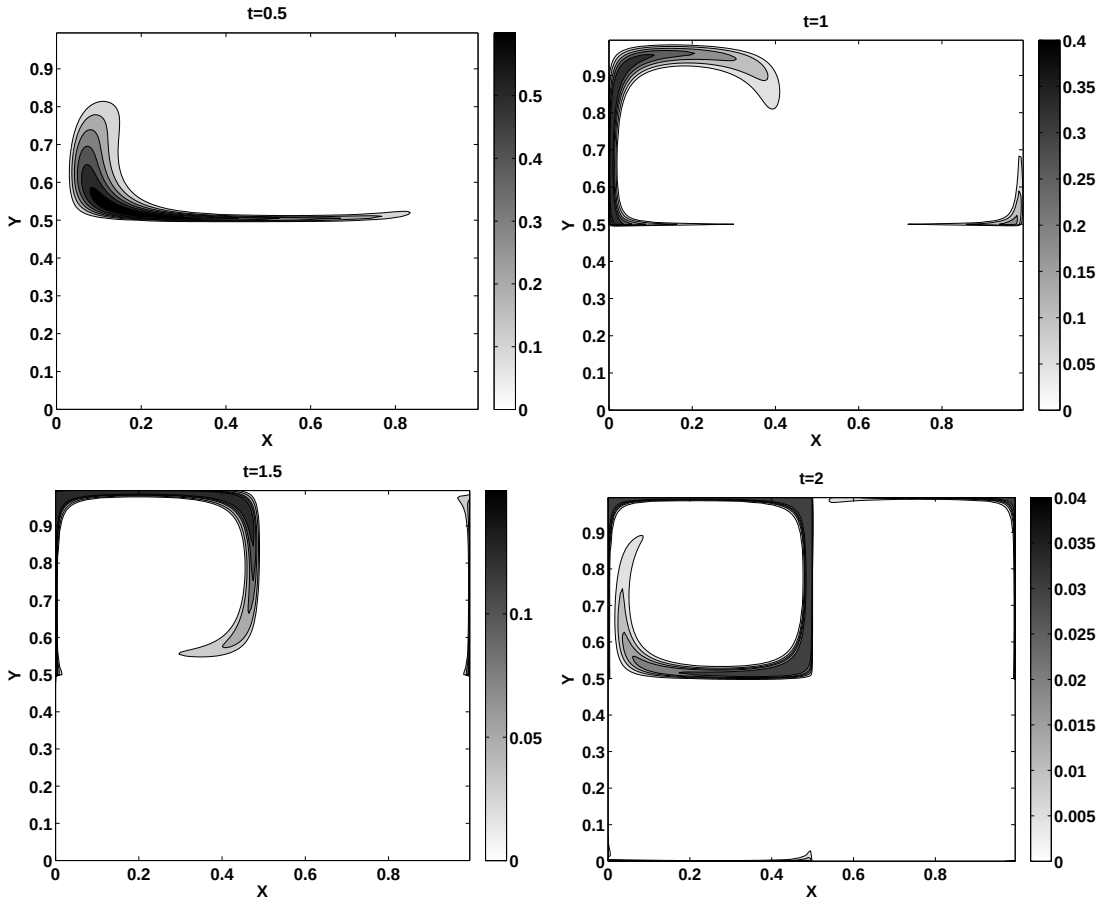

Figure 7: Results for spray dynamics dragged by the gas field made of Taylor-Green vortices, computed with the multi-fluid method for ten sections. Droplet mass at time $t = 0.5$ (top-left), $t = 1$ (top-right), $t = 1.5$ (bottom-left), $t = 2$ (bottom-right). The computation is carried out in a 100×100 grid.

The particle Stokes number of the distribution is initially 0.017 for the high order moment method, and ranges from 0.0028 to 0.045 for the multi-fluid model with ten sections. The spray evaporation rate is set as $K = 0.27$. Figures 6 and 7 show the evolution of the spatial mass distribution for both computation. Due to the cloud initial location, two parts of it are dragged by two different vortices. That is why the main part of the cloud is dragged in the top-left vortex, whereas a smaller part of the cloud is dragged in the top-right vortex. From [28, 7, 29], we know that there exists a critical value $\mathrm{St}_c = 1/8\pi$ (≈ 0.0398) which separates two regimes. For $\mathrm{St} < \mathrm{St}_c$, the particles cannot escape from the Taylor-Green vortices while, for $\mathrm{St} \geq \mathrm{St}_c$, they are ejected out of their original vortices. This explains that, with the multi-fluid method, a part of the mass is in the bottom vortices: Stokes number under consideration goes beyond St_c for the last sections. However, this is not captured by the high order moment method since only one averaged Stokes number is considered and is lower than St_c.

However, the general notice is that the level of comparison is very good. Indeed, results at $t = 0.5$

and $t = 1$ are very similar between the two methods. At time $t = 1.5$ and $t = 2$, the fact that the droplets are dragged faster in the case of the high order moment method comes from the computation of the drag term. In both models, the Stokes number writes $\theta\overline{S}$, where θ is defined in 2.2 and $\overline{S}$ is the average droplet surface of the distribution. In the case of the multi-fluid model, $\overline{S} = \frac{3}{5}(S_{i+1}^{5/2} - S_i^{5/2})/(S_{i+1}^{3/2} - S_i^{3/2})$ [24]. As indicated in Fig. 5-right, the sections with the highest mass are between 0.44 and 0.6, so that $\overline{S}$ is approximately 0.52. In the case of the the high order moment method, $\overline{S} = m_1/m_0 = 0,3487$. In terms of dynamics, our model only considers the particle mean velocity. Meanwhile, ten sections are considered for this case in the multi-fluid model, which amounts to ten different fluids with their own velocity. The spray dynamics conditioned on size is thus better resolved in the multi-fluid model. Nevertheless, in order to assess the accuracy of the models in terms of mean dynamics of the droplets, we have performed some studies on the evolution of the mean droplet size through evaporation. First, Fig. 8-left displays the evolution of the droplet mass through evaporation of a motionless cloud. It can be concluded that the multi-fluid model, with ten sections, is not as accurate as the high order moment method. Further comparisons and conclusions can be found in [30]. In a second study, the evolution of the mean particle size through evaporation, given by both the models, are compared. It can be seen in Fig. 8-right that the high order moment method is more accurate than the multi-fluid model in assessing the dynamical value of m_1/m_0. That means that, the term of mean drag, and thus the mean particle velocity is better solved by the high order moment method than the multi-fluid model. Remarkably enough, even with 40 sections, the multi-fluid model does not give as good results as the high order moment method. The conclusion to be drawn from the previous elements is that, even if the multi-fluid is able to capture the details of the dynamics conditioned on droplet size, the mean dynamics, for droplets below the critical Stokes number, is very well captured, even better captured, compared to the multi-fluid model. On the other hand let us recall that the accuracy of the description of the size distribution function is better in the high order moment method, this is discussed in [30].

Finally we would like to emphasize the fact that, to solve this problem, only six equations are solved in our model, whereas three equations per section are solved in the multi-fluid model, for a total of thirty equations, in two dimensions in space.

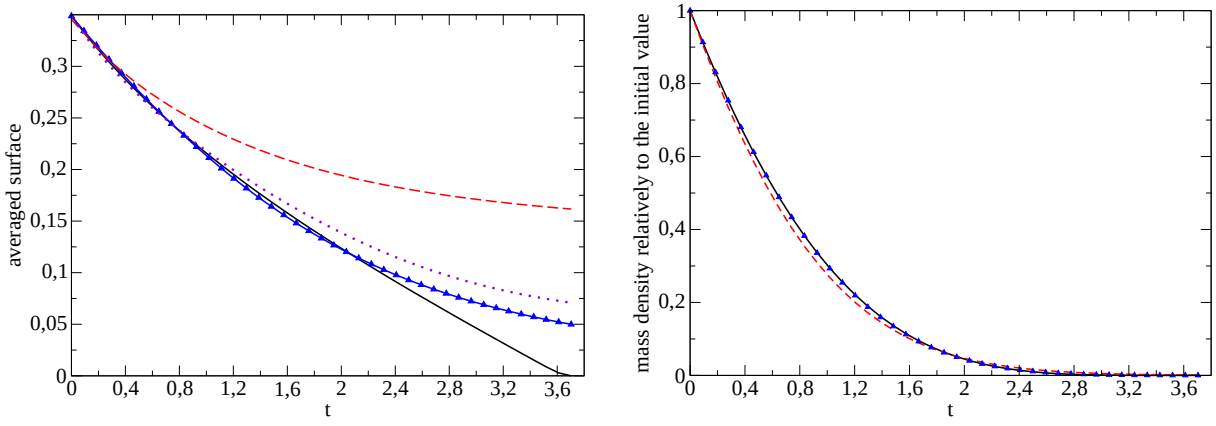

Figure 8: (Left) Evolution of the droplet mass of a motionless cloud through evaporation with a d^2 law, and comparison with the analytical solution. (Right) Evolution of the mean particle size through evaporation, and comparison with the analytical solution. Black solid curve: analytical solution; triangles: high order moment method; dashed red curve: multi-fluid model with ten sections; violet dots: multi-fluid model with 40 sections.

The critical question of time efficiency is addressed in a study comparing the computation time required for the high order moment method and for the multi-fluid model with ten sections, on the configuration described above. Three different computations have been performed, first on a 50, then on a 100×100 and finally on a 200×200 cell grid. For each computation, the total CPU time is assessed. Moreover, in order to evaluate the relative importance of the phase space and physical space transport, the time spent in each and every routine is recorded. Table 1 displays the results of the analysis on the

total computation time and the relative time spent for the resolution of transport in phase space and physical space, respectively. This analysis points out the time efficiency of the high order moment method (EMSM), which is about 4 times faster than the multi-fluid method (MF). This is a real achievement, given the quality of the comparison of the results. The second result provided is that the relative importance of phase space transport decreases as the number of cells increases. Moreover, Table 2 compares the number of variables solved for each operator resolution, for both models. For phase transport, six variables must be solved in the case of the high order moment method (the four size moments and the two components of the velocity), while f_{ME}, the reconstructed NDF is obtained from the moments by an iterative solver. On the other hand, three variables per section, the mass (denoted $m_{3/2}$ as it is proportional to the size moment of order 3/2) and the two components of the velocity, are explicitly solved in the case of the multi-fluid model, which amounts to thirty variables in total. For physical transport, six variables must be solved in the case of the high order moment method, whereas, the same thirty must be solved in the case of the multi-fluid model. It also gives the ratio between the computation time of the multi-fluid to the computation time of the high order moment method. Table 2 shows that the term for which the resolution is done with the biggest computation time difference between the two models is physical transport, i.e the multi-fluid (with ten sections) resolution lasts four times as long as the resolution with the high order moment method. Extrapolating from these results, we can legitimately expect that this ratio will become higher in three dimensions, and that our new method will be much faster than the multi-fluid model, especially since most of the computation time will be devoted to transport in physical space. We also notice that the phase space transport can easily be parallelized. As a result, our new method proves to be very attractive for three-dimensional configurations.

Grid	50×50			100×100			200×200		
	Phase	Physical	Total (s)	Phase	Physical	Total (s)	Phase	Physical	Total (s)
EMSM	49.6 %	50.4%	52	43%	57%	318	34.5%	65.5%	2140
MF	56.79%	43.21%	205	47.25%	52.75%	1269	38.39%	61.61%	8461
Ratio	4.5	3.4	3.9	4.4	3.7	4	4.4	3.7	3.9

Table 1: Computation time comparison between the high order moment method (MMS) and the multi-fluid method (MF). Phase denotes the relative time (in pourcent of the total time) spent for phase space transport (evaporation and drag). Physical denotes the relative time (in pourcent of the total time). Total denotes the total computation time (in seconds)

	EMSM	MF	Ratio time
Phase	$m_0, m_1, m_2, m_3, +f_{ME}$, u, v $= 6$ variables $+ f_{ME}$	$10 \times (m_{3/2}, u, v)$ $= 30$ variables	4.4
Physical	m_0, m_1, m_2, m_3, u, v $= 6$ variables	$10 \times (m_{3/2}, u, v)$ $= 30$ variables	3.6

Table 2: Comparison of the number of variables for the high order moment (MMS) and the multi-fluid (MF), for phase space and physical space transport. The last column represents the approximate ratio of the computational time spent for the multi-fluid model to the time spent for high order moment method, in the phase and physical transport respectively

5.3. Polydisperse evaporating spray in a turbulent free jet configuration

In this third test-case the high order moment method is assessed on a 2-D Cartesian weakly turbulent free jet. A polydisperse spray is injected in the jet core with the size distribution represented in Fig. 5-left. The simulations are conducted with an academic solver, coupling the ASPHODELE solver, developed at CORIA by Julien Reveillon and collaborators [36, 37], with the Eulerian solver MUSES3D [7, 29] developed at EM2C Laboratory, using the models and the numerical scheme presented in these article.

The ASPHODELE solver couples a Eulerian description of the gas phase with a Lagrangian description of the spray.

As far as the gas phase is concerned, a 2-D Cartesian low Mach number compressible solver is used. The gas jet is computed on a 400×200 uniformly spaced grid. To destabilize the jet, we inject turbulence using the Klein method with 10% fluctuations [23]. The Reynolds number based on U_0, ν_0 and L_0 is $1,000$, where U_0 is the injection velocity and L_0 is the jet width. Dimensional quantities for illustration purposes will be based on a velocity of $U_0 = 1$ m/s and $L_0 = 1.5 \times 10^{-2}$ m, with typical value of $\nu_0 = 1.6 \times 10^{-5}$ m^2/s. Finally we have $\rho_l/\rho_g = 580$. The gas vorticity is presented in Fig. 9.

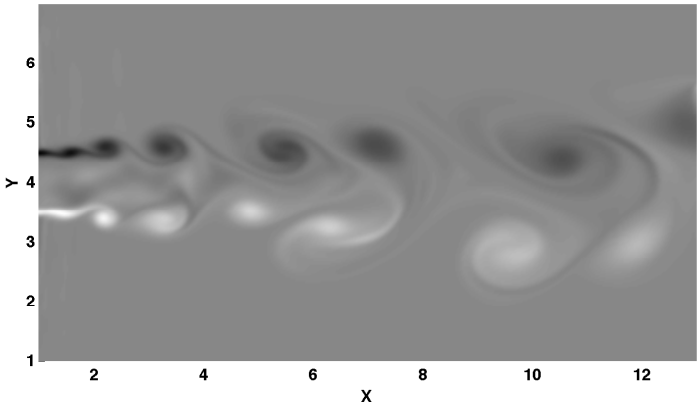

Figure 9: Free-jet configuration at time $t = 20$. Gas vorticity on a 400×200 grid.

As in the previous case studies, in order to validate the developments detailed in this article, two computations have been performed, one with our model and the second with the multi-fluid model. The efficiency of the multi-fluid model in describing polydisperse evaporating sprays has been demonstrated in [8, 22].

This free jet case is computed with an evaporating spray having an evaporation coefficient $K = 0.07$. The particle Stokes number is 0.275 for the high order moment method, corresponding to a diameter $d_0 = 75\mu m$, and ranges from St $= 0.047$ to St $= 0.75$ for the multi-fluid model with ten section, corresponding to diameters from $d_0 = 5\mu m$ to $d_0 = 85\mu m$. In order to correctly describe the evaporation process with the multi-fluid model, ten sections are considered, whereas only one section is required in the computation using the high order moment model. The computation runs until $t = 20$. Figure 10 displays the final mass fields for the spray. The level of comparison between the two resulting fields is very good. One can nevertheless notice a slight difference, i.e in the multi-fluid model with ten sections, the spray is less evaporated.

Since, our primary interest is in combustion applications, the paramount objective of evaporating spray modeling is prediction of the gas-phase fuel mass fraction. Therefore we present comparisons between the gas-phase fuel mass fraction obtained from the high order moment model and multi-fluid descriptions of the spray. These simulations were once again accomplished using one-way coupling. As a consequence, the evaporated fuel is not added as a mass source term in the gas-phase equations, but is stored in passive scalars for the gas. The two fields are plotted in Fig 11. These results confirm the quality of the previous results. The present comparison, by showing clear similarity between the two models, highlights the efficiency of the Eulerian high order moment model and the associated numerical schemes in describing polydisperse evaporating sprays. It has both the ability to cope with exactly zero droplet mass density and model singularities formation as well as the capability to propose an accurate Eulerian treatment of the polydisperse evaporating spray with a very limited amount of numerical diffusion such as the schemes developed for the multi-fluid model presented in [8, 22, 7, 18, 17].

These results are a first significant step towards combustion computations with full two-way coupling or flame dynamics in 3D such as the simulations presented in [18, 17] .

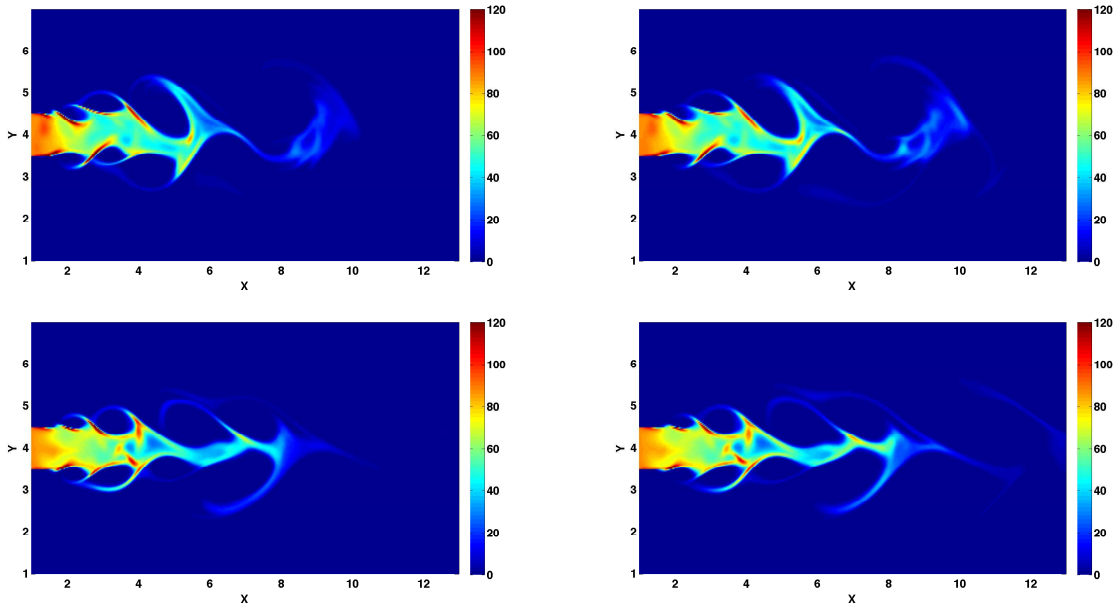

Figure 10: Total mass density of the polydisperse evaporating spray. (Top) Results at time $t = 15$. (Bottom) Results at time $t = 20$. (Left) High order moment method. (Right) Multi-fluid model with ten sections. The computation is carried out in a 400×200 grid

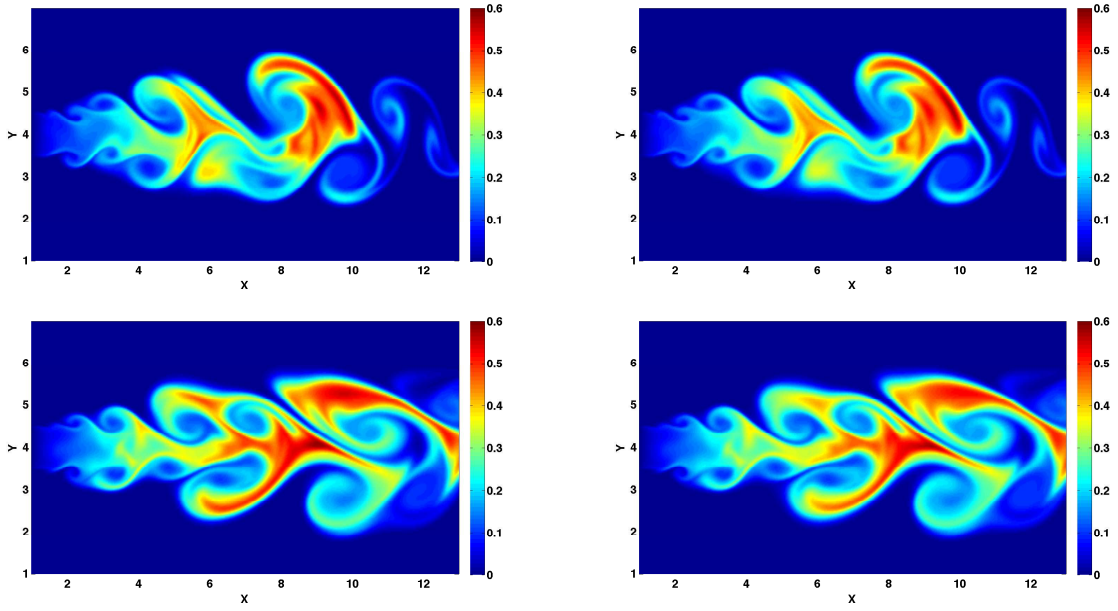

Figure 11: Comparison of the gas-phase fuel mass fraction. (Top) Results at time $t = 15$. (Bottom) Results at time $t = 20$. (Left) High order moment method. (Right) Multi-fluid model with ten sections. The computation is carried out in a 400×200 grid

6. Conclusion

The aim of this paper was to present a robust scheme which is capable of advecting size moments of a distribution function of an aerosol or a spray with a very low level of numerical diffusion. This issue is not

only limited to aerosols and sprays, but impacts every field where successive integer moment methods are involved. In this paper, we provide a viable, second order in space and time and cost-effective solution to this persistent problem which usually suffers from stability and realizability difficulties. This scheme has been devised using some algebra based on moment theory [10]. The moments are not the quantities which are directly transported. Instead we use the canonical moments which are much more easier to control, and allow the moment vector to stay in the moment space by transporting them separately. This method paves the way to better computing and explaining predictivity capacities of Eulerian models with respect to Lagrangian models.

Furthermore, it has been coupled with a method resolving droplet evaporation by an operator splitting algorithm, which shows the modularity of these operators. The proposed model and numerical methods can thus be easily coupled to a diffusion or break-up/coalescence model. The description of evaporation and advection of a polydisperse spray has been shown to be at least as accurate as the multi-fluid model in the mean, whereas the computational cost can thus be reduced substantially, all the more toward 3D simulations. It is important to notice the limitations of such an approach, since only one velocity field for the whole droplet range is considered: it will be very precise as long as the droplet Stokes number remain below the critical Stokes number associated to droplet crossing. For more inertial droplets, as presented in [30], we can consider several size intervals corresponding to similar droplet dynamics, the smaller one being devoted to the droplets with a Stokes number below the critical one. For more inertial droplets, we have to extend the model to droplet crossing trajectory.

This work thus enlightens an interesting perspective for the use of Eulerian models in the simulation of high Knudsen number spray, taking advantage of the work done in [14, 9, 16, 8, 22]. The ground idea is to use a high order moment method for velocity moments combined with quadrature method of moments (QMOM) such as recently done in [42] for droplets with Stokes numbers higher than the critical one. Eventually, a major achievement would be to reach high accuracy in a code, with the dual capability to account for evaporation of sprays, as well as take into account droplet trajectory crossings for more inertial droplets, while using the method presented in this contribution for the whole size range below the critical Stokes number where a single velocity has been shown to be accurate.

Acknowledgement

This research was supported by an IFP Energies Nouvelles/EM2C CIFRE Ph.D. grant for Damien Kah. The authors would like to thank J. Reveillon and H. Meftah for their help in designing the free jet configuration and for the use of the ASPHODELE Code developed in J. Reveillon's team at CORIA, Rouen, France. The help of S. de Chaisemartin is gratefully acknowledged in performing the numerical simulations of the free jet configuration with the multi-fluid model which he originally designed in his Ph.D. Thesis.

References

[1] F. Bouchut, *On zero pressure gas dynamics*, in Advances in kinetic theory and computing, vol. 22 of Ser. Adv. Math. Appl. Sci., World Sci. Publ., River Edge, NJ, 1994, pp. 171–190.

[2] F. Bouchut, S. Jin, and X. Li, *Numerical approximations of pressureless and isothermal gas dynamics*, SIAM J. Numer. Anal., 41 (2003), pp. 135–158.

[3] Y. Brenier and E. Grenier, *Sticky particles and scalar conservation laws*, SIAM Journal of Numerical Analysis, 35 (1998), pp. 2317–2328.

[4] C. Chalons, D. Kah, and M. Massot, *Beyond pressureless gas dynamics: quadrature-based velocity moment models*, Communication in Mathematical Sciences (submitted), (2010). available online at http://hal.archives-ouvertes.fr/hal-00535782/en/.

[5] S. Chandrasekhar, *Stochastic problems in physics and astronomy*, Rev. Mod. Phys., 15 (1943), pp. 1–89.

[6] S. Chapman and T. G. Cowling, *The mathematical theory of nonuniform gases*, Cambridge Mathematical Library, Cambridge University Press, Cambridge, third ed., 1990.

[7] S. de Chaisemartin, *Eulerian models and numerical simulation of turbulent dispersion for polydisperse evaporating sprays*, PhD thesis, Ecole Centrale Paris, France, 2009. Available online at http://tel.archives-ouvertes.fr/tel-00443982/en/.

[8] S. de Chaisemartin, L. Fréret, D. Kah, F. Laurent, R. Fox, J. Reveillon, and M. Massot, *Eulerian models for turbulent spray combustion with polydispersity and droplet crossing*, Comptes Rendus Mécanique, 337 (2009), pp. 438–448. (Special Issue Combustion for Aerospace Propulsion).

[9] S. de Chaisemartin, L. Fréret, D. Kah, F. Laurent, R. O. Fox, J. Reveillon, and M. Massot, *Eulerian models for turbulent spray combustion with polydispersity and droplet crossing: modeling and validation*, Proceedings of the Summer Program 2008, (2009), pp. 265–276.

[10] H. Dette and W. J. Studden, *The theory of canonical moments with applications in statistics, probability, and analysis*, Wiley Series in Probability and Statistics: Applied Probability and Statistics, John Wiley & Sons Inc., New York, 1997. , A Wiley-Interscience Publication.

[11] F. Doisneau, F. Laurent, A. Muronne, J. Dupays, and M. Massot, *Optimal eulerian model for the simulation of dynamics and coalescence of alumina particles in solid propellant combustion*, in Proceedings of the International Conference on Multiphase Flows, Tampa, Florida, 2010, pp. 1–15. available online at http://hal.archives-ouvertes.fr/hal-00498215/en/.

[12] F. Doisneau, F. Laurent, A. Murrone, J. Dupays, and M. Massot, *Evaluation of Eulerian Multi-Fluid models for the simulation of dynamics and coalescence of particles in solid propellant combustion*, J. of Comp. Physics (submitted), (2010).

[13] J. H. Ferziger and H. G. Kaper, *Mathematical Theory of transport processes in gases*, North-Holland, Amsterdam, 1972.

[14] R. O. Fox, *A quadrature-based third-order moment method for dilute gas-particle flow*, J. Comput. Phys., 227 (2008), pp. 6313–6350.

[15] R. O. Fox, F. Laurent, and M. Massot, *Numerical simulation of spray coalescence in an eulerian framework: direct quadrature method of moments and multi-fluid method*, Journal of Computational Physics, 227 (2008), pp. 3058–3088.

[16] L. Fréret, S. de Chaisemartin, F. Laurent, P. Vedula, R. O. Fox, O. Thomine, J. Reveillon, and M. Massot, *Eulerian moment models for polydisperse weakly collisional sprays: model and validation*, in Proceedings of the Summer Program 2008, Center for Turbulence Research, Stanford University, 2009, pp. 277–288.

[17] L. Fréret, S. De Chaisemartin, J. Reveillon, F. Laurent, and M. Massot, *Eulerian models and three-dimensional numerical simulation of polydisperse sprays*, in Proceedings of the International Conference on Multiphase Flows, Tampa, Florida, 2010, pp. 1–12. Available online at http://hal.archives-ouvertes.fr/hal-00498207/en/.

[18] L. Fréret, O. Thomine, J. Reveillon, S. de Chaisemartin, F. Laurent, and M. Massot, *On the role of preferential segregation in flame dynamics in polydisperse evaporating sprays*, in Proceedings of the Summer Program 2010, Center for Turbulence Research, Stanford University, 2010, pp. 1–10.

[19] S. K. Friedlander, *Smoke, Dust, and Haze, Fundamental of Aerosol Dynamics*, Topics in Chemical Engineering, Oxford University Press, second ed., 2000.

[20] H. Grad, *Principles of the kinetic theory of gases*, in Handbuch der Physik (herausgegeben von S. Flügge), Bd. 12, Thermodynamik der Gase, Springer-Verlag, Berlin, 1958, pp. 205–294.

[21] J. Greenberg, I. Silverman, and Y. Tambour, *On the origin of spray sectional conservation equations*, Combustion and Flame, 93 (1993), pp. 90–96.

[22] D. Kah, F. Laurent, L. Fréret, S. de Chaisemartin, R. Fox, J. Reveillon, and M. Massot, *Eulerian quadrature-based moment models for polydisperse evaporating sprays*, Flow, Turbulence and Combustion, 85 (2010), pp. 649–676. (Special Issue Dedicated to Stephen B. Pope).

[23] M. Klein, A. Sadiki, and J. Janicka, *A digital filter based generation of inflow data for spatially developing direct numerical or large eddy simulations*, J. Comput. Phys., 186 (2003), pp. 652–665.

[24] F. Laurent, *Numerical analysis of Eulerian multi-fluid models in the context of kinetic formulations for dilute evaporating sprays*, M2AN Math. Model. Numer. Anal., 40 (2006), pp. 431–468.

[25] F. Laurent and M. Massot, *Multi-fluid modeling of laminar poly-dispersed spray flames: origin, assumptions and comparison of the sectional and sampling methods*, Combust. Theory and Modelling, 5 (2001), pp. 537–572.

[26] R. J. LeVeque, *Finite volume methods for hyperbolic problems*, Cambridge Texts in Applied Mathematics, Cambridge University Press, Cambridge, 2002.

[27] D. L. Marchisio and R. O. Fox, *Solution of population balance equations using the direct quadrature method of moments*, Journal of Aerosol Science, 36 (2005), pp. 43–73.

[28] M. Massot, *Eulerian multi-fluid models for polydisperse evaporating sprays*, in Computational Models for Turbulent Multiphase Reacting Flows, vol. 492 of CISM Courses and Lectures, SpringerWienNewYork, Vienna, 2007, pp. 79–123. Editors D.L. Marchisio and R. O. Fox, Udine, July 2006.

[29] M. Massot, F. Laurent, S. de Chaisemartin, L. Fréret, and D. Kah, *Eulerian multi-fluid models: modeling and numerical methods*, in Modelling and Computation of Nanoparticles in Fluid Flows, Lectures Notes of the von Karman Institute, NATO RTO-EN-AVT-169, 2009. Available online at http://hal.archives-ouvertes.fr/hal-00423031/en/.

[30] M. Massot, F. Laurent, D. Kah, and S. de Chaisemartin, *A robust moment method for evaluation of the disappearance rate of evaporating sprays*, SIAM J. Appl. Math., (2010). In Press, http://hal.archives-ouvertes.fr/hal-00332423/en/.

[31] R. McGraw, *Numerical advection of correlated tracers: preserving particle size/composition moment sequences during transport of aerosol mixtures*, J. Phys.: Conf. Ser., 78 (2007), p. 5p.

[32] L. R. Mead and N. Papanicolaou, *Maximum entropy in the problem of moments*, J. Math. Phys., 25 (1984), pp. 2404–2417.

[33] H. Meftah, *Simulation Numérique Directe dun spray en évaporation : Analyse et modélisation du mélange turbulent et des transferts thermiques*, PhD thesis, INSA de Rouen, France, 2008.

[34] J.-B. Mossa, *Extension polydisperse pour la description euler-euler des écoulements diphasiques réactifs - TH/CFD/05/74*, PhD thesis, Institut National Polytechnique de Toulouse, 2005.

[35] D. Ramkrishna and A. G. Fredrickson, *Population Balances: Theory and Applications to Particulate Systems in Engineering*, Academic Press, 2000.

[36] J. Reveillon, *DNS of spray combustion, dispersion evaporation and combustion*, in Computational Models for Turbulent Multiphase Reacting Flows, vol. 492 of CISM Courses and Lectures, SpringerWienNewYork, Vienna, 2007, p. 229. Editors D.L. Marchisio and R. O. Fox, Udine, July 2006.

[37] J. Reveillon and F. Demoulin, *Effects of the preferential segregation of droplets on evaporation and turbulent mixing*, Journal of Fluid Mechanics, 583 (2007), pp. 273–302.

[38] G. Strang, *On the construction and comparison of difference schemes*, SIAM Journal of Numerical Analysis, 5 (1968), pp. 506–517.

[39] H. Struchtrup, *Macroscopic transport equations for rarefied gas flows*, Interaction of Mechanics and Mathematics, Springer, Berlin, 2005. Approximation methods in kinetic theory.

[40] F. A. Williams, *Spray combustion and atomization*, Phys. Fluids, 1 (1958), pp. 541–545.

[41] D. L. Wright, *Numerical advection of moments of the particle size distribution in Eulerian models*, Journal of Aerosol Science, 38 (2007), pp. 352–369.

[42] C. Yuan and R. O. Fox, *Conditional quadrature method of moments for kinetic equations*, Journal of Computational Physics (submitted), (2010).